Working with the ESEM at high temperature

Renaud Podor, G.I. Nkou Bouala, J. Ravaux, J. Lautru, Nicolas Clavier

Working with the ESEM at high temperature.

R. Podor*, G. I. Nkou Bouala, J. Ravaux, J. Lautru and N. Clavier

Institut de Chimie Séparative de Marcoule, UMR 5257 CEA/CNRS/ ENSCM/Univ Montpellier, Site de Marcoule, Bat 426, BP 17171, F-30207 Bagnols sur Cèze cedex

*Corresponding author. e-mail: renaud.podor@cea.fr

Keywords: High Temperature ; ESEM ; SEM ; in situ

Abstract

Working with the (Environmental) Scanning Electron Microscope (ESEM) at high temperature has been a long lasting goal for many researchers and remains to this day a difficult technique to operate efficiently. This article describes the properties of several different furnaces developed over the past 40 years, focusing specifically on the operation of the high temperature stage associated with the ESEM. Guidelines and advices for correct use of these systems are provided regarding the experience of the authors. A focus on sintering studies illustrates the main difficulties to implement this experimental technique.

Introduction

The first scanning electron microscope (SEM) was commercialized in 1965. This form of microscopy is a unique technique allowing the observation of materials at the nanometer scale with a high depth of field

while recording images at high magnifications. However, sample preparation requirements are stringent. Samples must be sufficiently conductive to prevent sample charging and stable under vacuum to be observed in a SEM, commonly making it only possible to observe post-mortem samples, i.e. not in situ. Very rapidly, groups of researchers have investigated the possibility of observing samples in the SEM chamber as if they were in their "natural" media – and/or under reactive conditions. The possibility to combine the observation of the sample surface (with a high spatial resolution) and the modifications of the sample morphology that can occur when submitted to environmental conditions remains to this day particularly attractive.

For the observation of wet materials, strategies to decrease the sample temperature and to inject water vapor on the sample have been developed to limit its dehydration and specific chambers that maintain a humid atmosphere around the sample have been built. Similarly, a series of furnaces have been designed to be integrated into a SEM chamber, originally with the aim to study the sintering of metallic or ceramic materials at high temperature. The first images have been reported by Fulrath from the Lawrence Berkeley Laboratory, University of California [1].

Parallel to this, the development of the environmental scanning electron microscope had begun in the late 70's with the works of Danilatos & Robinson [2]. The first ESEM was commercialized in 1988. This specific microscope (which was designed to work with a relatively high gas pressure in the main chamber) combines an original differential pumping system with electron detectors designed to work at high pressures (up to 750Pa). Custom stage holders were also developed since then. Among them, a 1500°C hot stage was patented in 1996 [3] along with a high temperature gaseous secondary electron detector. When combined into the ESEM, these systems offer a wide range of experimental conditions. Nowadays, most of the studies conducted at high temperature in a SEM are performed with this kind of high temperature stage.

This article will cover the different types of furnaces developed to be used in SEM equipment, focusing in detail on the furnace associated with the ESEM. Measurement of sample temperature as well as the most important parameters that must be adjusted to produce high quality images of materials at high temperature will be particularly emphasized. Finally, the capabilities of this technique will be highlighted through the example of sintering experiments recently reported in the literature.

Designing furnaces for high temperature experiments in the SEM

Heating the sample

When working with a conventional SEM, two types of electron detectors are available, i.e. Everhart-Thornley detector for the secondary electrons (SE) and conventional backscattered electron (BSE) detector which is commonly a semiconductor type. The conventional BSE detector is sensitive to light illumination, and as such, cannot be operated at high temperatures due to black body emission. Furthermore, if this type of BSE detector is located too close to the heat source, its semi conductive properties would be quickly lost. Thus, only the Everhart-Thornley detector can be used. In this case, only a high vacuum mode is possible (even in a low vacuum SEM). In most of the cases, furnaces that have been built work under vacuum and are coupled with the Everhart-Thornley detector.

One way to heat the sample locally in the SEM chamber is to use laser. This technique, called LASEM (Laser heating in the SEM chamber), was first developed and reported by Wetzig et al. [4]. In this system, the sample surface is directly heated by the laser beam to achieve steep temperature gradients in order to study a material's response to thermal shocks. Nevertheless, this heating mode requires precautions in order to protect the Everhart-Thornley detector from extreme thermal electron emission and limit gases emission from the specimen. Further developments of laser heating in the ESEM chamber combine advantages of both systems. The authors claim that temperatures as high as 1700°C can be reached

locally using high energy laser beams [5]. Another advanced model, where a sample holder is heated by the laser beam is reported by Kirch et al. [6]. It allows heating up to 1200°C and simultaneously observing large sample areas for EBSD patterns recording.

Most of the hot stages are heated by resistive effect. Different devices have been designed since the late 60's, going from very simple to complex systems. The simplest design consists in heating metal boats [7] or filaments [8,9,10] by a direct current. The heating elements are generally made of refractory metals such as rhenium, tantalum, tungsten or molybdenum [7]. This method allows reaching temperatures as high as 2500°C, when the sample is directly deposited in a heated rhenium boat. In these conditions, the size of the device is sufficiently small to reach the operating temperature within a short time [7]. As these systems can only be efficient under vacuum, some contamination can occur inside the SEM chamber. A derived system was developed by Charyshkin et al. to be used in an ESEM, under a H_2 or H_2/CH_4 residual atmosphere, in which the filament was used to heat a plate where the sample can be deposited (maximum temperature of the sample holder of 850°C for a filament temperature equal to 2000°C) [8]. More recently, Munz et al. have used this technique under a flow of water vapor in the ESEM chamber to generate a thermal gradient along a Ti wire and observed the effect of substrate temperature on the growth of titania nanowires[9].

More complex and versatile devices have been developed based on a metallic heating coil wound on a threaded insulating material core, corresponding to a more classical furnace design. The metallic coil is heated by a regulated direct current. The nature of materials used for the furnace assembly can differ from one author to another. Heating stages for conventional SEM (i.e. high vacuum systems) generally combine refractory metals with alumina (thoriated tungsten wire [1], tungsten wire [11,12], molybdenum (Brown & Hill, 1989), tantalum [13], kanthal [12]), molybdenum [14]or nickel [15] with pyrophyllite, platinum combined with a MgO holder [3] or commercial devices (30W capacity Watlow fire-rod – probably made of steel -encapsulated into a copper sample holder [11]) (Fig. 1). The furnace

heats the sample holder made of a metal foil (tungsten or platinum) on which the sample to be observed is deposited. Most of these hot stages are simply mounted in the SEM chamber and do not require any cooling system. However, the maximum temperature that can be reached is around 1000°C [11, 14, 16] but temperatures as high as 1450°C were reported by Gregori et al. for relatively short-term experiments [13]. When higher temperature or longer experiments are required, the hot stage must be cooled by an external liquid coolant [3, 12] in order to prevent the degradation of SEM inner parts (mainly detectors). Using such a hot stage, Podor et al. performed sintering experiments on refractory ceramics up to 1400°C for 8 hours [17,18].

**********Fig. 1 to be inserted here **********

Figure 1. Several types of furnaces dedicated to high temperature experiments in the SEM that have been developed since the 70's. a) The furnace has been designed by Brouillette et al. [7]. The sample is contained in a boat that can be heated up to 2500K. A thermionic electron suppression grid is placed between the sample and Everhart - Thornley detector to minimize the thermal electron signal contribution in the final image; b) Schematic experimental setup and build-in hot stage for in-situ experiments by Charyshkin et al. [8]; c) Heating stage and thermal electron filter designed by Nakamura et al. [10] ; d) Reactive Ti filament designed by Munz et al. [9]; e) Modified stage with the heating stage (Verma et al. [11]); f,g) Schematic view of the furnace developed by Cohen et al. [14] with a view of a heater unit; h) – 1500°C furnace developed by Gatan Company (H1005 furnace).

Temperature measurement

Accurately measuring the sample temperature in the hot stage is of critical importance for the quality and reproducibility of the experiments. In many of the heating systems previously described, large temperature gradients exist near the sample, and the zone where the temperature is homogeneous can

be relatively limited [9]. Furthermore, the presence of gases in the SEM chamber, and mainly its pressure and nature, will modify the thermal gradients and thermic conductivity of the hot stage. This will make the temperature measurement more difficult to achieve accurately [16]. Thus, the position of the temperature measurement system must be as close as possible to the sample (ideally in direct contact) [19]. One solution is to use – when possible - an optical pyrometer [5] and/or an infrared-sensitive camera [16, 9, 10]. This technique is generally associated with the filament heating system which generates severe temperature gradients. The second solution is to use a classical thermocouple made of two different metals. In this case, the thermocouple head must be placed as close as possible to the specimen. To achieve this goal, some authors have decided to weld the thermocouple on the sample holder [7] or directly on the sample [14, 16]. The head of the thermocouple can also be located in a hole in the specimen [20]. Another possibility is to attach the thermocouple to the mount as close as possible to the sample [13, 15, 16, 21], or trap it between the specimen and the heater [16]. However, as mentioned by Brown and Hill [16] and Podor et al. [19], conduction down the thermocouple leads may cool the point of contact. This can result into a limitation of the hot stage maximum temperature or to an additional uncertainty on the specimen temperature measurement (depending on the thickness and composition of the material separating the sample and the head of the thermocouple). Different authors have decided to put the sample directly in contact with the head of the thermocouple in order to avoid these difficulties [6, 12, 14, 19]. In this configuration, specific attention must be paid to the possible reactivity between the thermocouple leads or head with the specimen.

The measure of the sample temperature is generally calibrated by determining melting points of pure compounds [14, 15, 19] and alloys [14]. The measurement methods using thermocouples are accurate (temperature difference below 10°C in the 231-660°C temperature range, 2°C at 1000°C [14] and 5°C at 1064°C [15]). Brown and Hill have used three different systems (welded thermocouple to the specimen, optical and infrared pyrometry) and they underline that there is a good agreement between the three

measuring systems [16]. Some authors also underline the fact that if the head of the thermocouple is in direct contact with metallic samples, the recorded melting temperature can be up to 15°C lower than the expected temperature [1, 14].

In the specific montage built by Gregori et al. in which the thermocouple is located directly under the graphitic sample holder, the authors have noticed that there is a small deviation between the measured and the expected temperature on the specimen surface [13]. This deviation depends on the composition, thickness and porosity of the sample as well as on the maximum temperature, but can reach up to 40°C.

Collecting the electrons : secondary vs thermal electrons

The increase of the sample temperature yields to the generation and emission of thermal electrons. The emission intensity can be calculated by the Richardson law; the higher the temperature, the higher the thermal electron emission [22]. Thus, at high temperature, the thermo-ionic emission can be much more intense than the electron emissions resulting from the primary electron beam interaction with the sample [21]. As the SEM image contrasts are built by comparing the secondary (and/or backscattered) electrons emitted by different zones of the sample, the challenge is to separate the thermo-ionic emission from the secondary electron emission. If not, the quality of the images may be substantially deteriorated [7, 23]. Different strategies have been developed to discriminate the thermo-ionic electron emission from the secondary electron emission. First, the encapsulation of the heating wires reduces the thermo-ionic electron emission and it mainly contributes to improve the image quality [13]. Second, the nature of the sample holder can also influence the global thermal electron emission. Replacement of a MgO sample holder by a Pt one has allowed to decrease the thermo-ionic electron emission for a given temperature [21]. Third, the more generalized method consists in the energy filtering of both types of electrons using a suppression grid or a shielding system. Brouillette & Leyshon reported that the

suppression grid is biased with a potential adjusted to prevent thermionically emitted electrons from penetrating the grid and entering the collection field while at the same time permitting secondary electrons, which have higher energies, to enter the collection field [7]. The suppression grids are generally formed by a metal grid [3, 7, 10] and the shielding systems are made by a metal plate with apertures positioned above the specimen [13]. The shielding system also protects the SEM chamber from heat [3, 13] and / or the detectors from light emission [11, 14].

Introduction of gases

Depending on the type of SEM that is used, as well as on the nature of the heating element, the experiments can be performed under a gaseous environment. The gases can be injected near the sample via a gas handling vacuum line to observe specific processes [11, 20]. However, these gases must not be in contact with the heating element (if made of molybdenum or tungsten) if they are oxidizing. In this configuration, the precise control of the gas partial pressure near the sample is difficult and can be estimated [24] or calculated [16]. In every case, the determination of the gas pressure near the sample depends on the system geometry as well as the nature of the gas.

The development of the ESEM in the 80's has offered new opportunities. Among them, it has been specifically designed to allow working at precisely controlled gas pressures in the sample chamber. When working at high temperature, the gas pressure around the sample typically ranges between 10 to 750Pa. Thus, coupling this microscope with a specific hot-stage equipped with a platinum made heating element allows experiments under reducing, neutral or oxidizing gases to be performed. The gases that were used are H_2O, O_2, H_2, CH_4, C_2H_2, CH_3CH_2OH, He or gas mixtures, but this list is not exhaustive.

The heating assembly associated with the ESEM

The heating assembly associated with the ESEM contains a dedicated furnace, heat shield and gaseous secondary electron detector. This system will now be described in detail and the general guidelines to work with this integrated system will be reviewed.

A dedicated heating stage

The furnace associated with the ESEM has been developed by Hardt and Knowles and patented in 1996 [3]. A general scheme of this furnace is reported on Fig. 2. In this device, the sample is directly placed on the sample holder which can be made from carbon (for reductive atmospheres) or Pt-coated MgO (for reductive, neutral and oxidizing conditions). The sample holder is inserted in the center of the specimen heater assembly (zone 1 on Fig. 2a). In this assembly, the heating element is a wound heater wire coil which is positioned close to the sample cup. It is usually made of an iron-based alloy, or of platinum, depending on the maximum temperature of the furnace (1000 and 1400°C respectively). The heating element is embedded into an insulating high temperature ceramic in order to avoid electrical contacts between the different parts of the wire and/or with the specimen, and to limit the heat loss. This assembly is packed into a larger insulating ceramic (Zone 2 on Fig. 2a) that is maintained into a metallic envelope (Zone 6 on Fig. 2a). This envelope contains a water cooling system which limits radiant heat loss in the ESEM chamber (Fig. 2a).

**********Fig. 2 to be inserted here **********

Figure 2: High temperature stage provided by FEI Company to be installed in the ESEM. a) Schematic view of the inner parts of the furnace [3]. b) The HT stage is placed in the ESEM chamber with the heat

shield and the high temperature GSE detector. c) A series of images recorded when heating the sample at room temperature, 1150, 1250 and 1280°C.

Sample biasing

In order to limit the amount of thermal electrons in the total electron signal to be collected, a bias voltage ranging between +50V and -50V can be applied to the sample holder in the original assembly. The electrical continuity between the biased platinum wire and the sample is ensured by a platinum coating that is deposited on the sample holder. Thermal and secondary electrons have different energies. Typically, the energy of the thermal electrons is lower than 1eV while the energy of the secondary electrons is around a few tens of eV [7, 10]. Thus, sample biasing can act differently on each emission depending on its value. When biasing the sample positively, the sample bias acts as a filter: thermal electrons are attracted to the substrate (and they are trapped) while the secondary electrons can still be emitted to the detector. Thus, both signals are separated. When biasing the sample negatively, the energy of both thermal and secondary electrons is increased and the efficiency of the gas amplification is also increased for the most energetic electrons. Thus, the contribution of the secondary electron emission in the total collected signal is increased. In this case, sample bias acts as a differential amplifier of both signals. Playing with sample bias generally yields to an increase of the image contrast. However, the adjustment of this parameter remains tricky and mainly related with a trial and error method.

A dedicated heat shield

In order to avoid radiant heat loss, a heat shield is installed in the specimen chamber above the specimen heating assembly (Fig. 2b). This heat shield includes a central opening to permit the electron beam to pass through and strike the sample. The heat shield assembly includes a series of thin ceramic insulating shields which act as heat reflectors and limit the heating inside the SEM chamber. A metal grid is also included in the heat shield. It can be biased up to 250V relative to the sample holder in order to accelerate secondary electrons emanating from the surface of the specimen to pass through the central opening of the heat shield assembly. The intensity of the bias required mainly depends on the sample temperature and it will be necessary to adjust this parameter continuously during the sample heating.

A dedicated gaseous secondary electron detector

A specific electron detector has been built on the basis of the Gaseous Secondary Electron Detector (GSED) used in the ESEM. The modified electron detector is in the form of a metallic thin ring electrode. In order to enhance image quality, the final pressure limiting aperture can be biased at a different voltage compared to the bias applied to the thin ring electrode. In addition, the bias voltage applied to the final pressure limiting aperture can float to provide automatic compensation. This specific detector is not sensitive to the light emitted during the heating of the sample (Fig. 2c).

The GSED (also called GDD for gaseous detection device) allows the formation of images in the conditions of an electron microscope and in the presence of gas inside the specimen chamber. As described by Danilatos, the SE and BSE signals emanating from the electron beam/specimen interaction interact with the surrounding gas in the form of gaseous ionization and excitation, resulting in their multiplication through 'electron avalanche' [25]. When attracted to the biased detector (20-500V), the emitted “gaseous electrons” signal is amplified and the number of gaseous electrons that are generated remains proportional to the intensity of the initial SE+BSE signals. This allows the formation of

"electronic" images. In parallel, the generated cations go onto the negatively charged surface to compensate the local sample surface charging effects. This effect allows the observation of insulating samples (Fig. 3a,b,c).

Measuring the sample temperature

Accurate and reproducible measurement of the sample temperature is a key point in achieving high temperature experiments. The initial high temperature stage provided by the FEI Company contains an integrated thermocouple that is located relatively far from the sample (embedded in the insulating ceramic, outside the heater – close to point 3 on Fig. 2a). Using this device, systematic measurement of the melting point of gold yielded to much disperse data. Thus, Podor et al. have developed a specific sample holder containing an integrated thermocouple on which the sample is positioned directly above [19]. This system allows a precise measurement of the sample temperature, independent of the furnace geometry and the nature and pressure of the gas that is used. However, when this thermocouple is used, the sample cannot be biased and the thermal electron filtering is more difficult at high temperature.

Performing in situ experiments with the heating stage of the ESEM

One of the main interests of performing in situ experiments in the ESEM is to monitor continuously the morphological modifications of the sample surface by constantly observing it at the same location. That is to say that the zone of interest must always be maintained in the field of view of the microscope during the heat treatment. This often requires continuous adjustment of many parameters affecting the recording of high quality images (heat shield bias, beam centering, image focus, stigmator…) i.e. that contain sufficient information to describe the phenomena at the scale at which the changes occur. In

other words, the image magnification must fit well with the morphological modifications to be observed. During HT-ESEM experiments, the main objective of the microscopist will be to record image series on the same zone of the sample with the same magnification and focus. The time between two images must be as short as possible if the sample morphological modifications are fast.

General guidelines to choose the best operating conditions when using the HT-ESEM are provided in the following part of this tutorial.

Choice of the sample

The size of the sample to be studied must be adjusted with the requirements of the observations to be made. Several cases must be distinguished:

1) The sample is not a powder and the morphological modifications only occur at the sample surface and the inner part of the sample is not modified (oxidation of a superalloy for example). In this case, the sample can be relatively large. The only requirement is that it must fit within the sample holder (typically inserted into a 5mm diameter circle).
2) The sample is not a powder and the morphological modifications modify the bulk of the sample (sintering of a green pellet for example). In this case, the size of the sample can be strongly modified during the heat treatment and the region to be observed can shift during the observation. In order to limit the sample drift during the experiment, the sample must be as small as possible - typically 100-500 µm in length and 50-100 µm in height (but these values can be lowered).
3) The sample is a powder. In this case, the size of the sample must also be minimized and if necessary, the powder can be dispersed on a thin plate in order to observe the grains independently (a particular care must be taken to avoid chemical reactivity of the powder with

the substrate). Indeed, the heat treatment can change the organization of the grains and the zone to be observed can be lost. Furthermore, observing the sample with the electron beam can also yield to a dispersion of the powder due to electrical charging effects.

The choice of the sample size is not obvious and this is one of the main parameters that will guarantee the success of the HT experiments in the ESEM.

**********Fig. 3 to be inserted here **********

Figure 3. a) Skirting effect (The Gaussian curve illustrates the electron distribution of the primary electron beam at the sample surface). b) SE (and BSE) amplification in the gas. c) GSE concentration and collection using the heat shield and the GSE detector. d) Parameters to be adjusted to obtain images at high temperature in the HT-ESEM.

Making images in the HT-ESEM in the presence of gases

Almost 12 different and interdependent parameters must be adjusted, sometimes continuously or simultaneously, during the experiment, to obtain images at high temperature in the ESEM. These parameters and their links with the high temperature assembly are reported in Fig. 3d. The choices of some parameters are directly driven by the experimental conditions (temperature, nature and pressure of the gas), the sample itself and the expected magnification to observe the sample modifications. All these parameters must be adjusted in order:

- To minimize the skirting effect that is due to the scattering of primary electron beam in the gas remaining in the chamber,

- To optimize the signal/noise ratio of the electron (SE and BSE) collection regarding the sensitivity of the sample to the primary electron beam and the expected image resolution,
- To maximize the SE+BSE electron signal relative to the thermo-ionic emission,
- To perform the experiments in the expected conditions (temperature, nature and pressure of the gas).

First of all, the working distance, i.e. the distance between the final lens and the sample surface, cannot be lowered below 19 mm, due to the size and relative positions of the detector, the heat shield, the furnace and of the position of the sample inside the furnace. Thus, when considering the classical parameters used in conventional SEMs, this working distance is much higher than usual and it is not optimal for obtaining good quality images. In the high temperature assembly, this parameter is considered as a fixed parameter.

Generally, the high voltage of the primary electron beam is maximized to 30kV in order to limit the skirting effect of the electron beam through the gas present between the final lens and the sample surface. This value can be lowered if the sample is sensitive to the electron beam. The spot size and the intermediate diaphragm have to be adjusted to optimize the signal / noise ratio and the resolution of the images.

The nature and the pressure of the gas inside the ESEM chamber will impact both the primary electron beam skirting, the amplification of the gaseous second electron signal and image resolution. When increasing the gas pressure, the skirting is increased as well as the amplification of the gaseous second electron signal. However, when the pressure is too high (typically more than 400-500Pa water vapor or air), the skirting effect becomes very intense. Thus, the number of primary electrons that interact with the sample is low, the image resolution is decreased and the signal/noise ratio of the GSED is also decreased (see Stokes for more information [26]).

When the sample temperature increases (typically above 1150°C), the thermo-ionic signal becomes more and more intense. The energy of the thermal electrons (around 20~30eV) is generally lower than the secondary electron energy (less than a few eV) [10]). Thus, this electron emission can be partially filtered from the SE (and BSE) emissions that provide the information on the sample morphology. This filtering can be obtained by applying either positive or negative bias to the sample. When the sample bias is positive, the trajectories of the thermal electrons are deviated and they are attracted to the sample surface. As the energy of the thermal electrons remains lower than the secondary electron energy, both signals can be filtered (Fig. 3b). When the sample bias is negative, the electrons are accelerated and this energy increase favors the electron / gas molecule interactions. As the energy of SE is higher than that of thermal electrons, this additional energy is sufficient to increase the gas ionization due to the SE and to enhance this signal rather than the background due to the thermal electrons. Furthermore, when the sample holder developed by Podor et al. is placed inside the furnace, the sample cannot be biased and there will be no help in the filtering of the thermal electrons [19].

The heat shield bias must be adjusted to concentrate and to direct the electron signal to the GSE detector as a function of the sample temperature:

- When the sample temperature is below 350-500°C, biasing of the heat shield is inefficient on the image quality. In this condition, the presence of the heat shield in the trajectory of the electrons to the detector leads the number of collected electrons to decrease. Thus, the quality of the images remains low below 500°C. One possibility is to remove the heat shield when working at low temperature.
- On the contrary, when the temperature is higher than 500°C, biasing the heat shield above 200V yields to an increase of the GSE signal and to an improvement of the image quality. This effect remains efficient up to 1100-1200°C, depending on the nature of the gas and on the pressure that are used.

- At higher temperatures (1200-1350°C), the thermo-ionic emission becomes very intense and the GSE signal over the noise generated by this additional emission is very low. Thus, the quantity of electrons to be directed to the GSE detector must be lowered, and it is necessary to decrease the heat shield bias. In parallel, it is also necessary to adjust continuously the GSED parameters by decreasing the brightness, contrast and enhance values in order to avoid detector saturation.
- When the temperature is higher than 1350°C, the formation and stabilization of the images become very tricky. As the parameters associated to the GSED, as well as the heat shield bias, are generally optimized at this point, it is impossible to change them. Thus, it could be necessary to decrease the gas pressure in order to reduce the GSE generated by the gas amplification. Last, if the intensity of the SE+BSE signals is too low compared to the thermo-ionic emission, the signals of interest must be enhanced by increasing the intensity of the primary electron beam. This will lower the image resolution but remains the only way to improve the quantity of information available on the recorded images. This is generally combined with the modification of the parameters associated with the images (contrast, brightness and gamma). In this temperature domain, the increase of the experimental temperature yields important changes in the relative intensities of the different electronic emissions. Thus, the adjustments of all the imaging parameters must be done between each image, yielding to an increase of the time necessary to record an image.

The main conditions required to obtain images at high temperature are summarized on Fig. 4. The range quoted for ideal gas pressures (50-400Pa) is a general guideline for most of the conventional gases (air, water vapor…). The limits of the range can vary depending on the nature of the gas and the gas amplified electron emission currents [25, 27, 28].

**********Fig. 4 to be inserted here **********

Fig. 4. Summary of the main required conditions to obtain images at high temperature using the high temperature associated with the ESEM.

The specific case of experiments performed under high vacuum

When the experiment is performed under high vacuum, the SE signal is directly collected using the Everhart-Thornley detector. In this particular case, the heat shield must not be used to direct the electrons to the GSE detector but only to help extracting the secondary electrons and partly filtering the thermal electrons. The heat shield bias is ranging between 2-20V and must be adjusted continuously with increasing temperature. Thus, as the SE trajectory must be deviated to the detector, it is also necessary to leave a sufficient gap between the heat shield and the furnace to let the electrons go to the detector: the working distance should be increased by 1 - 2 millimeters.

Unexpected difficulties and further advices

Unexpected difficulties could occur due to different reasons:

- Additional vibrations on the images can be due to the water cooling system of the furnace. They can limit the maximum magnification achievable by the microscope.

- The surface of the sample can be contaminated by the formation of impurities due to the reactivity of the sample with the furnace, the sample holder, ceramics, impurities or residues of previous experiments.
- Unexpected reactions with the gases can occur and modify the morphology of the sample surface.
- Important modifications of the sample morphology can occur during the heat treatment at high temperature. They can yield to a loss of the region of interest by an important drift of the sample.

Some specific advices can be given to future HT-ESEM users. To avoid the sample surface contamination from one experiment to another one, it must be necessary:

- To change as regularly as necessary the ceramics of the furnace and of the heat shield. It can be necessary to change them between each experiment.
- To take a particular care of the experiments that generate pollutants that can be deposited in the cold parts of the heating assembly and that can yield to further degradation of the assembly when heating at higher temperature or under different reducing/oxidizing conditions.
- To take care of the experiments performed under H_2. Indeed, this gas reacts with platinum (heater of the heating element) to form platinum hydrides. After platinum hydrides decomposition, porosities are formed in the heater that becomes fragile and can break easily. Furthermore, one must take into account that particular safety caution must be employed by using H_2 gas.
- To take care of the experiments where the sample reacts with the gas – oxidation of a metal performed in air as an example. Indeed, even if there is a continuous renewal of the gas in the ESEM chamber generated by the entry of gas balanced with removal of gas to maintain vacuum, this renewal remains very low (a few cubic centimeters per minute (as the chamber volume is

approximately 30 liters for a Quanta 200 or XL30) and it cannot be controlled and regulated. Thus, in this case, the partial pressure of oxygen in the ESEM chamber will decrease – as there is no controlled renewal of the atmosphere in the ESEM chamber - and the experimental conditions will not remain the same all along the experiment.

- To outgas the furnace under high vacuum before the experiments when necessary (particularly to decrease the partial pressure of oxygen or to remove traces of water).

Sintering of ceramics: an example of experiments performed at high temperature in the ESEM

High temperature ESEM can address very different types of scientific topics such as sintering, chemical reactivity, oxidation, grain growth, etc. The case of experiments dedicated to the study of ceramic sintering and performed recently with the HT-ESEM will now be reported.

The use of HT-SEM for the study of sintering of ceramics has been one of the main reason for the development of the first furnaces adapted to the SEM chamber [1, 29, 30, 31]. The first attempts to achieve the observation of sintering in the ESEM have been reported in 2002 by Srinivasan [12] and later by Mazargui & Cutard [32] and Subramaniam & Roseman [22]. In these studies, the magnification of the images remained below 5000 times. Problems related with sample contamination / degradation at high temperature are reported by Subranamiam, which prevent the sintering of the material that is studied [33]. In 2006-2007, Klemensoe et al. and Nakagawa et al. have observed microstructural changes in a Ni - Yttria Stabilized Zirconia at high temperature during redox cycling [34, 35]. In 2011, Courtois et al. have reported the sintering of lead phosphovanadate in the temperature range 500-700°C [36]. In this study, a strong effect of the electron beam on the sintering temperature – and kinetic - is reported. The authors concludes that “ESEM equipped with a hot-stage furnace is really a powerful tool to provide information

on sintering but determination of the local temperature and the true role of electric field should receive more attention to be entirely conclusive". In parallel, Jolly-Pottuz et al. have developed a specific strategy to limit the effect of thermal emission on the image quality at high temperature. Images were recorded up to 1375°C, and the formation of necks between grains has been observed directly in the ESEM chamber [21]. However, these authors report that "it was not always straightforward to correlate sintering experiments performed in situ inside the microscope and sintering experiments performed ex situ in a classical oven used to prepare ceramics materials". In all these studies, the precise observation – and description – of the sintering process (through grain growth as an example) is generally limited by the image resolution and / or by the time step between two images that is relatively long.

Since 2010, we are developing specific strategies for the observation of the different stages of sintering of ceramic materials using the HT-ESEM. All the experiments are performed using a FEI Quanta 200 ESEM FEG equipped with a HT1500 hot stage provided by the FEI Company. The design of these experiments often requires the preparation of specific samples, sometimes the development of adapted image processing procedures and the results are systematically compared with those obtained by other techniques.

First of all, one must report that in some particular cases, contamination of the sample surface or reactivity of the sample with the substrate (material of the sample holder) has been observed. In the first example (Fig 5a), the formation of precipitates at the sample surface was associated both with the nature of the ceramics that are used to build the HT1500 stage by the FEI Company and with a contamination of the ceramics that were used to protect the heat shield during previous experiments. As previously reported, to overcome these difficulties, the ceramics of the heat shield have to be changed regularly.

In the second example, the reactivity of sample holders with the samples was observed. This phenomenon is mainly due to the presence of trace elements in the platinum that is used. Thus, particular specimen holders that are stable in the temperature range of the experiment, not chemically reactive with the sample and with the furnace, are now used (Fig 5b).

**********Fig. 5 to be inserted here **********

Fig. 5. a) Contamination of the sample's surface due to the partial degradation of the ceramics included in the HT1500 stage (T=1400°C). b) Chemical reactivity of the sample holder (FKS – Y_2O_3 stabilized platinum alloy) with the sample (CeO_2) at T=1200°C.

The first direct and continuous observation of grain growth during the third stage of CeO_2 sintering using HT-ESEM was reported by Podor et al. [17, 18]. The time step between two images was typically ranging between 5 and 30 seconds, and the magnifications that were used allowed to observe grains smaller than 30nm long. Images were systematically recorded on the same zone of the sample, in order to be able to characterize precisely the sintering process, and more particularly phenomenon that are generally not observable (motion of the grain boundaries, variation of the grain size, pore elimination) by conventional techniques [17, 18]. The displacement of the sample during the sintering process remained limited because small size samples (500µm long maximum) were used (Fig. 6a). These samples were cut directly from a unique green pellet. The same type of experiment has also been performed with ThO_2 in the temperature range 1250-1400°C using the same procedure for the sample's preparation [37]. The dwell time for these experiments was 8 hours after reaching the sintering temperature.

Observing the first stage of ceramics sintering has also been achieved by developing a specific analytical procedure. The main aim was to duplicate the "two-sphere" model that is classically used for the modelling of the first stage of sintering [38]. 100-500nm diameter microspheres of CeO_2 and ThO_2 have

been synthesized, then deposited on Pt (or Pt-Au5) sample holders (Fig. 6b). Both CeO_2 and ThO_2 were further studied between 1000 and 1275°C [39, 40].

**********Fig. 6 to be inserted here **********

Fig. 6. a) Image of a sample that is used for the study of the intermediate and third stage of sintering. b) Image of the CeO_2 microspheres after deposition on the PtAu5 sample holder. The arrow indicates the position of the system of interest.

Typical image series that have been recorded during the study of CeO_2 and ThO_2 sintering are reported in figure 7a, b, c and d. The resolution of the images, as well as the short time step between two images, are sufficient to measure precisely the grain size, neck size, angle between the grain, on the one hand, and grain size, length of grain boundaries as well as relative positions of the grain boundaries, on the other hand. From all these datasets, a huge quantity of original experimental data was collected. They were systematically compared with similar data obtained from the conventional techniques used for the study of sintering (including dilatometry and density measurements), or even modelling, when available [41]. No discrepancy between the different datasets has been reported, indicating that there was no beam effect during the experiments performed into the ESEM chamber.

**********Fig. 7 to be inserted here **********

Fig. 7. a) Image series of CeO_2 microspheres at T=1100°C during the study of the first stage of sintering. b) Image series of CeO_2 grains at T=1100°C during the study of the intermediate and final stage of sintering. c) Image series of ThO_2 microspheres at T=1250°C during the study of the first (and second) stage of sintering. d) Image series of ThO_2 grains at T=1250°C during the study of the intermediate and

final stage of sintering. The times that are inserted refer to the duration of the experiment since the beginning of the heat treatment at isothermal temperature.

Conclusions and outlooks

To conclude, here is a summary of the advice suggested in order to achieve high quality images whilst performing HT-ESEM experiments:

1) This technique is complex and requires a long-term training in order to use the microscope efficiently and produce the best data possible. The main objective of this training is to able to record high quality images in the required experimental conditions. Thus, the first piece of advice is to listen to the microscopist!

2) *Before* analysis, the end-user must discuss with microscopist the specific phenomena that will be studied. Understanding the problem will allow the microscopist to define the working conditions more precisely.

3) The sample must be prepared correctly according the sample type in order to observe the morphological modifications of the sample surface accurately.

4) The experimental conditions must be defined taking into account all the details that will help to obtain a good set of data:

- Which sample holder must be used?
- In which conditions must the experiment be performed (temperature, nature of the gas, pressure…),
- Beam conditions (high voltage, expected beam current, diaphragms, detectors…),

- What can modify the sample observation (sensitivity of the sample to the electron beam, reactivity with gases, phase change during the experiment…),
- Expected magnification(s),
- Time delay between two images to be recorded, total number of images, contrast, brightness, enhance parameters thinking “image processing” and not only “sample observation”.

5) It is often necessary to perform a preliminary experiment to determine at which conditions (temperature, pressure etc) any surface transformations will occur and what experimental conditions will optimize the collection of data at these points.

After the experiments, the most difficult – and time consuming - part of the work begins. First of all, a dedicated strategy for image processing should be systematically adapted to the image series that have been recorded and to the kinetic parameters that are studied. Second, the interpretation of the data / results is generally not obvious as the observation of the morphological changes of a sample is not always easy to correlate to conventional thermal analyses processes.

Within the last twenty years, this technique has been widely used in many different technical domains of materials chemistry and physics of materials. Among them, one can cite the oxidation of materials [42, 43, 44, 45, 46, 47], healing and self-healing [48, 49, 50, 51], dewetting [52, 53, 54, 55, 56], reactivity (chemical reactivity, synthesis…) [9, 57, 58, 59, 60, 61, 62], crystallization [63, 64, 65, 66], energy [67, 68], phase change [69, 70, 71], soldering (and welding / joining) [72], decomposition of materials [73, 74, 75, 76], corrosion [77, 78]. This list is not exhaustive and the stages attached to the (E)SEM are now coupling mechanical testing with high temperature. The future of this technique would be probably driven by emerging applications such as SOFC, catalysis, which require to increase the gas pressure surrounding the sample and to mimic the operando conditions.

Recent works exhibit original advances and applications of high temperature SEM that can draw guidelines for future developments. EBAC (Electron Beam Absorbed Current)) images have been recorded at high temperature, opening the possibility to observe samples with a high resolution under gaseous atmospheres at high temperature [79].In parallel, topographic reconstructions and acquisition of 3D surface images at high temperature has also been achieved recently [77, 80] (Figure 8a, b). Last, a new design of furnace directly derived from the heating cells built for TEM [81, 82] has been recently implemented in a SEM. The experiment is reported in a pioneering work by Fanta et al. [54]. These authors have mounted MEMS heating chips in an in house designed TKD holder to study thin-film dewetting processes. The obtained data allow combining STEM-in-SEM imaging with local crystallographic data while heating the sample. Another research group is also developing such chip-based in situ heating device to investigate phase transformation phenomena in thin films [83].

These last developments clearly illustrate the technical and scientific potentials of this technique and what could drive future developments of high temperature SEM. However, coupling a high temperature stress with the precise control of the composition of the gas surrounding the sample remains the best way to reproduce or simulate operando conditions. Today, this can be achieved only with a scanning electron microscope operating under variable pressure with various gases.

**********Fig. 8 to be inserted here **********

Fig. 8. a) SEM view of a crystal formed at 850°C in a ceramic-glass. b) Topographic reconstruction of a glass ceramic during cristallisation recorded at T=850°C [78].

References

[1] R.M. Fulrath, Scanning Electron Microscopy to 1600°C. SEM (1972), Chicago (Illinois), 17–24. https://www.osti.gov/biblio/4627284-scanning-electron-microscopy-sup.
[2] G.D. Danilatos, V.N.E. Robinson, Principles of scanning electron microscopy at high specimen pressures, Scanning 2 (1979) 72-82. https://doi.org/10.1002/sca.4950020202.
[3] R.W. Knowles, T.A. Hardt, High temperature specimen stage and detector for an environmental scanning electron microscope. Patent n°WO 97/07526 (1996). https://patentscope.wipo.int/search/en/detail.jsf?docId=WO1997007526.
[4] K. Wetzig, J. Edelmann, W. Fischer, H. Mueller, LASEM - A novel combined device for laser modification in SEM, Scanning 9 (1987) 99-107, https://doi.org/10.1002/sca.4950090303.
[5] A.H. Foitzik, M.W. Füting, G. Hillrichs, L.J. Herbst, In situ laser heating in an environmental scanning electron microscope, Scanning 19 (1997) 119-124. https://doi.org/10.1002/sca.4950190211.
[6] D.M. Kirch, A. Ziemons, T. Burlet, I. Lischewski, X. Molodova, D.A. Molodov, G. Gottstein, Laser powered heating stage in a scanning electron microscope for microstructural investigations at elevated temperatures, Rev. Sci. Instrum. 79 (2008) 043902. https://doi.org/10.1063/1.2908434.
[7] J.W. Brouillette, W.E. Leyshon, Hot sub-stage for a scanning electron microscope. US patent n°3919558 (1975). https://patents.google.com/patent/US3919558.
[8] E. Charyshkin, N.N. Kinaev, M. Waterworth, D.R. Cousen, N. Calos, T. Bostrom, A. Ilyushechkin, In-situ electron microscopy studies of hot filament chemical vapour deposition diamond thin film growth in an environmental SEM, Phys. status solidi A 154 (1996) 43-54. https://doi.org/10.1002/pssa.2211540106.
[9] M. Munz, M.T. Langridge, K.K. Devarepally, D.C. Cox, P. Patel, N.A. Martin, G. Vargha, V. Stolojan, S. White, R.J. Curry, Facile synthesis of titania nanowires via a hot filament method and conductometric measurement of their response to hydrogen sulfide gas, ACS Appl. Mater. Interfaces 5 (2013) 1197-1205. https://pubs.acs.org/doi/abs/10.1021/am302655j.
[10] M. Nakamura, T. Isshiki, M. Tamai, K. Nishio, Development of a new heating stage equipped thermal electron filter for scanning electron microscopy. Proc. 15th International Congress on Electron Microscopy Durban (South Africa) (2002). https://atomic.es.kit.ac.jp/~knishio/presentation/ICEM15/ICEM15_Nakamura.pdf.
[11] S.K. Verma, G.M. Raynaud, R.A. Rapp, Hot-stage scanning electron microscope for high-temperature in-situ oxidation studies, Oxid. Met. 15 (1981) 471-483. https://link.springer.com/article/10.1007/BF00603538.
[12] N.S. Srinivasan, Dynamic study of changes in structure and morphology during the heating and sintering of iron powder, Powder Technol. 124 (2002) 40-44. https://doi.org/10.1016/S0032-5910(01)00478-8.
[13] G. Gregori, H.J. Kleebe, F. Siegelin, G. Ziegler, In situ SEM imaging at temperatures as high as 1450°C, J. Electron Microsc. 51 (2002) 347-352. https://academic.oup.com/jmicro/article/51/6/347/896244.
[14] J.M. Cohen, K.J. Hartle, M.B. Waldron, A simply constructed heating stage for the SEM, J. Microsc. 118 (1980) 463-470. https://doi.org/10.1111/j.1365-2818.1980.tb00296.x.

[15] M.M. Rebbeck, I. Sikorski, A simple inexpensive heated specimen stage for the scanning electron microscope, J. Phys. E-Sci. Instrum. 21 (1988) 1106-1107. http://iopscience.iop.org/article/10.1088/0022-3735/21/11/023/pdf.
[16] A.M. Brown, M.P. Hill, A hot stage SEM for gas-solid reaction studies, J. Microsc. 153 (1989) 51-62. https://onlinelibrary.wiley.com/doi/pdf/10.1111/j.1365-2818.1989.tb01466.x.
[17] R. Podor, N. Clavier, J. Ravaux, L. Claparède, N. Dacheux, D. Bernache-Assollant, Dynamic aspects of cerium dioxide sintering: HT-ESEM study of grain growth and pore elimination, J. Eur. Ceram. Soc. 32 (2012) 353-362. https://doi.org/10.1016/j.jeurceramsoc.2011.08.032.
[18] R. Podor, N. Clavier, J. Ravaux, L. Claparède, N. Dacheux, In situ HT-ESEM observation of CeO_2 grain growth during sintering, J. Am. Ceram. Soc. 95 (2012) 3683-3690. https://doi.org/10.1111/j.1551-2916.2012.05406.x.
[19] R. Podor, D. Pailhon, J. Ravaux, H.P. Brau, Development of an integrated thermocouple for the accurate sample temperature measurement during High Temperature Environmental Scanning Electron Microscopy (HT-ESEM) experiments, Microsc. Microanal. 21 (2015) 307-312. https://doi.org/10.1017/S1431927615000252.
[20] J.E. Castle, M.R. Hunt, In-situ oxidation of iron and steel in the scanning electron microscope, Corros. Sci. 16 (1976) 137-142. https://doi.org/10.1016/0010-938X(76)90054-8.
[21] L. Joly-Pottuz, A. Bogner, A. Lasalle, A. Malchere, G. Thollet, S. Deville, Improvements for imaging ceramics sintering in situ in ESEM, J. Microsc. 244 (2011) 93-100. https://doi.org/10.1111/j.1365-2818.2011.03512.x.
[22] C. R. Crowell, The Richardson constant for thermionic emission in Schottky barrier diodes, Solid-State Electronics. 8(4) (1965) 395–399. https://doi.org/10.1016/0038-1101(65)90116-4.
[23] S. Subramaniam, R. Roseman, In situ observation of sintering behavior in barium titanate using an environmental scanning electron microscope, in: C.B. Di Antonio (Ed.), Characterization and modeling to control sintered ceramic microstructures and properties, Ceramic transactions 157 (2005) 97-104. https://doi.org/10.1002/9781118407080.ch11.
[24] A.M. Brown, P.L. Surman, Oxidation of iron within the scanning electron microscope: oxide crystallite growth kinetics during the oxidation of iron in CO_2, Surf. Sci. 52 (1975) 85-102. https://doi.org/10.1016/0039-6028(75)90010-2.
[25] G.D. Danilatos, Theory of the Gaseous Detector Device in the ESEM, Advances in Electronics and Electron Physics 78 (1990) 1-102. https://doi.org/10.1016/S0065-2539(08)60388-1.
[26] D.J. Stokes, Principles and practice of variable pressure/environmental scanning electron microscopy (VP/ESEM), John Wiley & Sons Ltd, The Atrium, Southern Gate, Chichester, West Sussex, UK, 2008.
[27] A.L. Fletcher, B.L. Thiel, A.M. Donald, Amplification measurements of alternative imaging gases in environmental SEM, J. Phys. D: Appl. Phys. 30 (1997) 2249-2257. http://iopscience.iop.org/article/10.1088/0022-3727/30/15/018.
[28] T.W. Sharley, F. Bonnie, J. Scott, M. Toth, Role of gas molecule complexity in environmental scanning electron microscopy and photoelectron yield spectroscopy, ACS Appl. Mater. Interfaces 8 (2016) 27305-27310. https://pubs.acs.org/doi/abs/10.1021/acsami.6b08681.
[29] C.B. Shumaker, R.M. Fulrath, Initial Stages of Sintering of Copper and Nickel, in: G. C. Kuczynski (Ed.), Sintering and Related Phenomena, Mater. Sci. Res. 6 (1973) 191-199. https://link.springer.com/chapter/10.1007/978-1-4615-8999-0_14.

[30] D.J. Miller, SEM Hot Stage Sintering of UO_2. Master thesis, University of California, Berkeley (1976). https://inis.iaea.org/collection/NCLCollectionStore/_Public/08/289/8289667.pdf?r=1&r=1.
[31] D.N.K. Wang, Sintering of Al_2O_3 powder compact by HT-SEM. PhD Thesis, University of California, Laurence Berkeley Laboratory (1976)
[32] H. Marzagui, T. Cutard, Characterisation of microstructural evolutions in refractory castables by in situ high temperature ESEM, Journal of Materials Processing Tech. 155-156 (2004) 1474-1481. https://doi.org/10.1016/j.jmatprotec.2004.04.365.
[33] S. Subramaniam, In Situ High Temperature Environmental Scanning Electron Microscopic Investigations of Sintering Behavior in Barium Titanate. PhD thesis, University of Cincinnati (2006). https://etd.ohiolink.edu/pg_10?133840530588776::NO:10:P10_ETD_SUBID:81159.
[34] T. Klemensoe, C.C. Appel, M. Mogensen, In situ observations of microstructural changes in SOFC anodes during redox cycling, Electrochem. Solid State Lett. 9 (2006) A403-A407. doi: 10.1149/1.2214303.
[35] Y. Nakagawa, K. Yashiro, K. Sato, T. Kawada, J. Mizusaki, Microstructural changes of Ni/YSZ cermet under repeated redox reaction in Environmental Scanning Electron Microscope (ESEM), Electrochem. Soc. Trans. 7(1) (2001) 1373-1380. http://ecst.ecsdl.org/content/7/1/1373.abstract.
[36] E. Courtois, G. Thollet, L. Campayo, S. Le Gallet, O. Bidault, F. Bernard, In situ study of the sintering of a lead phosphovanadate in an Environmental Scanning Electron Microscope, Solid State Ionics 186 (2011) 53-58. https://doi.org/10.1016/j.ssi.2011.01.004.
[37] N. Clavier, R. Podor, L. Delière, J. Ravaux, N. Dacheux, Combining in situ HT-ESEM observations and dilatometry: an original and fast way to the sintering map of ThO_2, Mater. Chem. Phys. 137(3) (2013) 742-749. https://doi.org/10.1016/j.matchemphys.2012.10.003.
[38] R.L. Coble, Initial Sintering of Alumina and Hematite, J. Am. Ceram. Soc. 41 (1958) 55-61. https://doi.org/10.1111/j.1151-2916.1958.tb13519.x.
[39] G.I. Nkou Bouala, N. Clavier, J. Léchelle, S. Martin, N. Dacheux, J. Favrichon, H.P. Brau, R. Podor, From in situ HT-ESEM observations to simulation: how does polycristallinity affects the sintering of CeO_2 microspheres?, *J. Phys. Chem. C* **120** (2016) 386-395. https://pubs.acs.org/doi/abs/10.1021/acs.jpcc.5b10465.
[40] G.I. Nkou Bouala, N. Clavier, J. Léchelle, J. Monnier, Ch. Ricolleau, N. Dacheux, R. Podor, High-Temperature Electron Microscopy Study of ThO_2 Microspheres Sintering, J. Eur. Ceram. Soc. 37(2) (2017) 727-738. https://doi.org/10.1016/j.jeurceramsoc.2016.08.029.
[41] M. Ajdour, J. Lechelle, F. Valdivieso, P. Goeuriot, K. Saikouk, R. Boyer, Sintering simulation at a scale lower than the grain size, Adv. Sci. Technol. 45 (2006) 516-521. https://www.scientific.net/AST.45.516.
[42] K. Kameya, O. Lee, Soot cake oxidation on a diesel particulate filter: Environmental Scanning Electron Microscopy observation and thermogravimetric analysis, Energy Technol. 1, (2013) 695-701. https://doi.org/10.1002/ente.201300103.
[43] N. Nasani, Z.J. Wang, M.G. Willinger, A.A. Yaremchenko, D.P. Fagg, In-situ redox cycling behaviour of Ni-$BaZr_{0.85}Y_{0.15}O_{3-d}$ cermet anodes for protonic ceramic fuel cells, Int. J. Hydrogen Energ. 39 (2014) 19780-19788. https://doi.org/10.1016/j.ijhydene.2014.09.136.

[44] C. Gasparrini, R. Podor, M. Pettina, D. Horlait, R. Chater, L. Vandeperre, W.E. Lee, Maltese Cross formation and oxidation of zirconium carbide, *Oxid. Met*. 88 (2017) 509-519. https://link.springer.com/article/10.1007/s11085-016-9672-6.
[45] C. Gasparrini, R. Podor, D. Horlait, M.J.D. Rushton, O. Fiquet, W.E.Lee, Oxidation of UC: an in situ high temperature environmental scanning electron microscopy study, J. Nucl. Mater. 494 (2017) 127-137. https://doi.org/10.1016/j.jnucmat.2017.07.016.
[46] H.A. Mehedi, J. Ravaux, K. Yazda, T. Michel, S. Tahir, M. Odorico, R. Podor, V. Jourdain, Increased chemical reactivity of single-walled carbon nanotubes on oxide substrates: In situ imaging and effect of electron and laser irradiations, Nano Research 9 (2016) 517-529. https://link.springer.com/article/10.1007/s12274-015-0933-5.
[47] T. Perez, L. Latu-Romain, R. Podor, J. Lautru, Y. Parsa, S. Mathieu, M. Vilasi, Y. Wouters, In-situ oxide growth characterization of Mn-containing Ni-25Cr (wt.%) model alloys at 1050°C, Ox. Met. 89(5) (2018) 781-795. https://link.springer.com/article/10.1007/s11085-017-9819-0.
[48] B.A. Wilson, E.D. Case, In situ microscopy of crack healing in borosilicate glass, J. Mater. Sci. 32 (1997) 3163-3175. https://link.springer.com/content/pdf/10.1023/A:1018698600884.pdf.
[49] D. Coillot, F.O. Méar, R. Podor, L. Montagne, L. Autonomic self-repairing glassy materials, Adv. Funct. Mater. 20 (2010) 4371-4374. https://doi.org/10.1002/adfm.201000147.
[50] V. Doquet, N. Ben Ali, E. Chabert, F. Bouyer, Experimental and numerical study of crack healing in a nuclear glass, Mech. Mater. 80 (2015) 145-162. https://doi.org/10.1016/j.mechmat.2014.09.003.
[51] S. Castanié, T. Carlier, F.O. Méar, S. Saitzek, J.F. Blach, R. Podor, L. Montagne, Self-healing glassy thin coating for high temperature application, ACS Appl. Mater. Interfaces 8(2) (2016) 4208-4215. https://pubs.acs.org/doi/10.1021/acsami.5b12049.
[52] M. Wada, Observation of dynamic image of Pt/Ti thin film at high temperature by in situ FE SEM, J. Japan Inst. Metals 73(12) (2009) 943-947. https://doi.org/10.2320/jinstmet.73.943.
[53] P. Jacquet, R. Podor, J. Ravaux, J. Teisseire, I. Gozhyk, J. Jupille, R. Lazzari, Grain growth: key in understanding silver solid-state dewetting, Scripta Mater. 115 (2016) 128-132. https://doi.org/10.1016/j.scriptamat.2016.01.005.
[54] P. Jacquet, R. Podor, J. Ravaux, J. Lautru, J. Teisseire, I. Gozhyk, J. Jupille, R. Lazzari, On the influence of oxygen on solid-state dewetting of polycristalline silver thin films, Acta Mater. 143 (2018) 281-290. https://doi.org/10.1016/j.actamat.2017.08.070.
[55] A.B. Fanta, M. Todeschini, A. Burrows, H. Jansen, C.D. Damsgaard, H. Alimadadi, J.B. Wagner, Elevated temperature transmission Kikuchi diffraction in the SEM, Mater. Charact. 139 (2018) 452-462. https://doi.org/10.1016/j.matchar.2018.03.026.
[56] S. W. Hieke, M.-G. Willinger, Z. J. Wang, G. Richter, D. Chatain, G. Dehm, C. Scheu, On pinning-depinning and microkink-flow in solid state dewetting: Insights by in-situ ESEM on Al thin films, Acta Mater. 165 (2019) 153-163. https://doi.org/10.1016/j.actamat.2018.11.028
[57] H. Boucetta, R. Podor, S. Schuller, L. Stievano, J. Ravaux, X. Carrier, S. Casale, S. Gossé, A. Monteiro, Mechanism of RuO_2 crystallization in simplified borosilicate containment glass: an original in situ ESEM approach, Inorg. Chem. 51(6) (2012) 3478-3489. https://pubs.acs.org/doi/abs/10.1021/ic202156y.
[58] P.R. Kidambi, B.C. Bayer, R. Blume, Z.J. Wang, C. Baehtz, R.S. Weatherup, M.G. Willinger, R. Schloegl, S. Hofmann, Observing graphene grow: catalyst−graphene interactions during scalable

graphene growth on polycrystalline copper, Nano. Lett. 13(10) (2013) 4769-4778. https://pubs.acs.org/doi/10.1021/nl4023572.
[59] Z.J. Wang, G. Weinberg, Q. Zhang, T. Lunkenbein, A; Klein-Hoffmann, M. Kurnatowska, M. Plodinec, Q. Li, L. Chi, R. Schloegl, M.G. Willinger, Direct observation of graphene growth and associated copper substrate dynamics by in situ Scanning Electron Microscopy, ACS Nano 9(2) (2015) 1506-1519. https://pubs.acs.org/doi/10.1021/nn5059826.
[60] H.A. Mehedi, J. Ravaux, S. Tahir, R. Podor, V. Jourdain, In situ study of single-walled carbon nanotube growth in an environmental scanning electron microscope, Nanotechnology 27 (2016) 505701. http://iopscience.iop.org/article/10.1088/0957-4484/27/50/505701.
[61] M. Niania, R. Podor, S.J. Skinner, J.A. Kilner, In-situ surface analysis of SOFC cathode degradation using high temperature Environmental Scanning Electron Microscopy, ECS Transactions 68(1) (2015) 665-670. http://ecst.ecsdl.org/content/68/1/665.abstract.
[62] M. Niania, R. Podor, T.B. Britton, C. Li, S. Cooper, N. Svetkov, S. Skinner, J. Kilner, In-situ study of strontium segregation in LSCF in ambient atmospheres using HT-ESEM, J. Mater. Chem. A 6 (2018) 14120-14135. https://pubs.rsc.org/en/content/articlehtml/2018/ta/c8ta01341a.
[63] M. Hillers, G. Matzen, E. Véron, M. Dutreilh-Colas, A. Douy, Application of in situ high-temperature techniques to investigate the effect of B_2O_3 on the crystallization behavior of aluminosilicate E-Glass, J. Am. Ceram. Soc. 90(3) (2007) 720–726. https://doi.org/10.1111/j.1551-2916.2006.01469.x.
[64] C. Bocker, M. Kouli, G. Volksch, C. Russel, New insights into the crystallization of cordierite from a stoichiometric glass by in situ high-temperature SEM, J. Mater. Sci. 49 (2014) 2795-2801. https://link.springer.com/article/10.1007/s10853-013-7984-3.
[65] J. Huguet-Garcia, A. Jankowiak, S. Miro, D. Gosset, R. Podor, F. Meslin, Y. Serruys, J.M. Costantini, In-situ E-SEM and TEM observations of the thermal annealing effects on ion-amorphized 6H-SiC and nanophased SiC fibers, Phys. status solidi B 1 (2015) 149-152. https://doi.org/10.1002/pssb.201400139.
[66] H. Vigouroux, E. Fargin, B. Le Garrec, M. Dussauze, V. Rodriguez, F.Adamietz, J. Ravaux, R. Podor, S. Lotarev, V. Sigaev, D. Vouagner, D. De Ligny, B. Champagnon, In situ study of the crystallization mechanism in $LiNbO_3$–SiO_2 glasses, Phys. Chem. Glasses: Eur. J. Glass Sci. Technol. B 54(2) (2013) 84–88. http://www.ingentaconnect.com/content/sgt/ejgst/2013/00000054/00000002/art00003.
[67] S.D. Beattie, G.S. McGrady, Hydrogen desorption studies of $NaAlH_4$ and $LiAlH_4$ by in situ heating in an ESEM, Int. J. Hydrogen Energ. 34 (2009) 9151-9156. https://doi.org/10.1016/j.ijhydene.2009.09.033.
[68] J. Huguet-Garcia, A. Jankowiak, S. Miro, R. Podor, E. Meslin, L. Thome, Y. Serruys, J.M. Costantini, Characterization of the ion-amorphization process and thermal annealing effects on third generation SiC fibers and 6H-SiC, EPJ Nuclear Sci. Technol. 1 (2015) 1-8. https://doi.org/10.1051/epjn/e2015-50042-9.
[69] S. Fischer, K. Lemster, R. Kaegi, J. Kuebler, B. Grobéty, B. (2004). In situ ESEM observation of melting silver and Inconel on an Al_2O_3 powder bed, J. Electron Microsc. 53(4) (2004) 393-396. https://doi.org/10.1093/jmicro/dfh070.

[70] L. Sanchez-Silva, J.F. Rodrıguez, M. Carmona, A. Romero, P. Sanchez, Thermal and Morphological Stability of Polystyrene Microcapsules Containing Phase-Change Materials, J. Appl. Polym. Sci. 120 (2011) 291–297. https://doi.org/10.1002/app.33112.
[71] F. Pedraza, R. Podor, Influence of annealing conditions on the formation of hollow Al_2O_3 microspheres studied by in situ ESEM, Mater. Charact. 113 (2016) 198-206. https://doi.org/10.1016/j.matchar.2016.01.018.
[72] Y.H. Kim, K.T. Kim, S.Y. Shin, S.I. Kwun, Effect of Additive Powder on Microstructural Evolution in the Wide-gap Brazed Region by In-situ High Temperature ESEM, Adv. Mater. Res. 26-28 (2007) 535-537. https://www.scientific.net/AMR.26-28.535.
[73] C.F. Blanford, C. Barry Carter, A. Stein, In situ high-temperature electron microscopy of 3DOM cobalt, iron oxide, and nickel, J. Mater. Sci. 43 (2008) 3539-3552. https://link.springer.com/article/10.1007/s10853-008-2550-0.
[74] N. Hingant, N. Clavier, N. Dacheux, S. Hubert, N. Barré, R. Podor, L. Aranda, Preparation of morphology controlled $Th_{1-x}U_xO_2$ sintered pellets from low temperature precursors, Powder Technol. 208 (2011) 454–460. https://doi.org/10.1016/j.powtec.2010.08.042.
[75] M. Castagna, E. Goergen, K. Skinner, J.E. Dahl, Utilization of an ESEM™ with an embedded heating stage to investigate pyrolosis in immature oil shale, Microsc. Microanal. 20(3) (2014) 1642-1643. https://doi.org/10.1017/S1431927614009945.
[76] N. Clavier, J. Maynadié, A. Mesbah, J. Hidalgo, R. Lauwerier, G.I. Nkou Bouala, S. Parrès-Maynadié, D. Meyer, N. Dacheux, R. Podor, Thorium aspartate tetrahydrate precursor to ThO_2: comparison of hydrothermal and thermal conversions, J. Nucl. Mater. 487 (2017) 331-342. https://doi.org/10.1016/j.jnucmat.2017.02.035.
[77] B. Schmid, N. Aas, Ø. Grong, R. Ødegård, In situ environmental scanning electron microscope observations of catalytic processes encountered in metal dusting corrosion on iron and nickel, Appl Catal A-Gen 215 (2001) 257-270. https://doi.org/10.1016/S0926-860X(01)00539-7.
[78] T. Jonsson, B. Pujilaksono, S. Hallström, J. Ågren, J.E. Svensson, L.G. Johansson, M. Halvarsson, An ESEM in situ investigation of the influence of H_2O on iron oxidation at 500°C, Corrosion Sci. 51 (2009) 1914-1924. https://doi.org/10.1016/j.corsci.2009.05.016.
[79] W. Joachimi, M. Hemmleb, U. Grauel, Z.J. Wang, M.G. Willinger, G. Moldovan, High temperature BSE and EBAC electronics for ESEM, Microsc. Microanal. 24 (1) (2018) 694-695. https://doi.org/10.1017/S1431927618003963.
[80] T. Carlier, F.O. Méar, S. Saitzek, R. Desfeux, J.F. Blach, R. Podor, L. Montagne, Crystallization mechanism of BaO-CaO-$Al2O_3$-SiO_2 glass thin films. 12th International Symposium on Crystallization in Glasses and Liquids, 10-13th September 2017, Segovia (Spain). http://secv.es/crystallization2017/web/pdf/Crystallization_2017.pdf.
[81] https://denssolutions.com/products/wildfire/
[82] https://www.protochips.com/products/fusion/
[83] E. Spiecker, C. Dolle, P. Schweizer, P. Denninger, Scanning transmission electron microscopy and diffraction in SEM: Novel approaches for in situ studies. CISCEM 2018 (10-12 oct 2018, Saarbrucken, Germany). http://www.ciscem2018.de/wp-content/uploads/sites/7/2018/09/180917-program-CISCEM-2018.pdf.

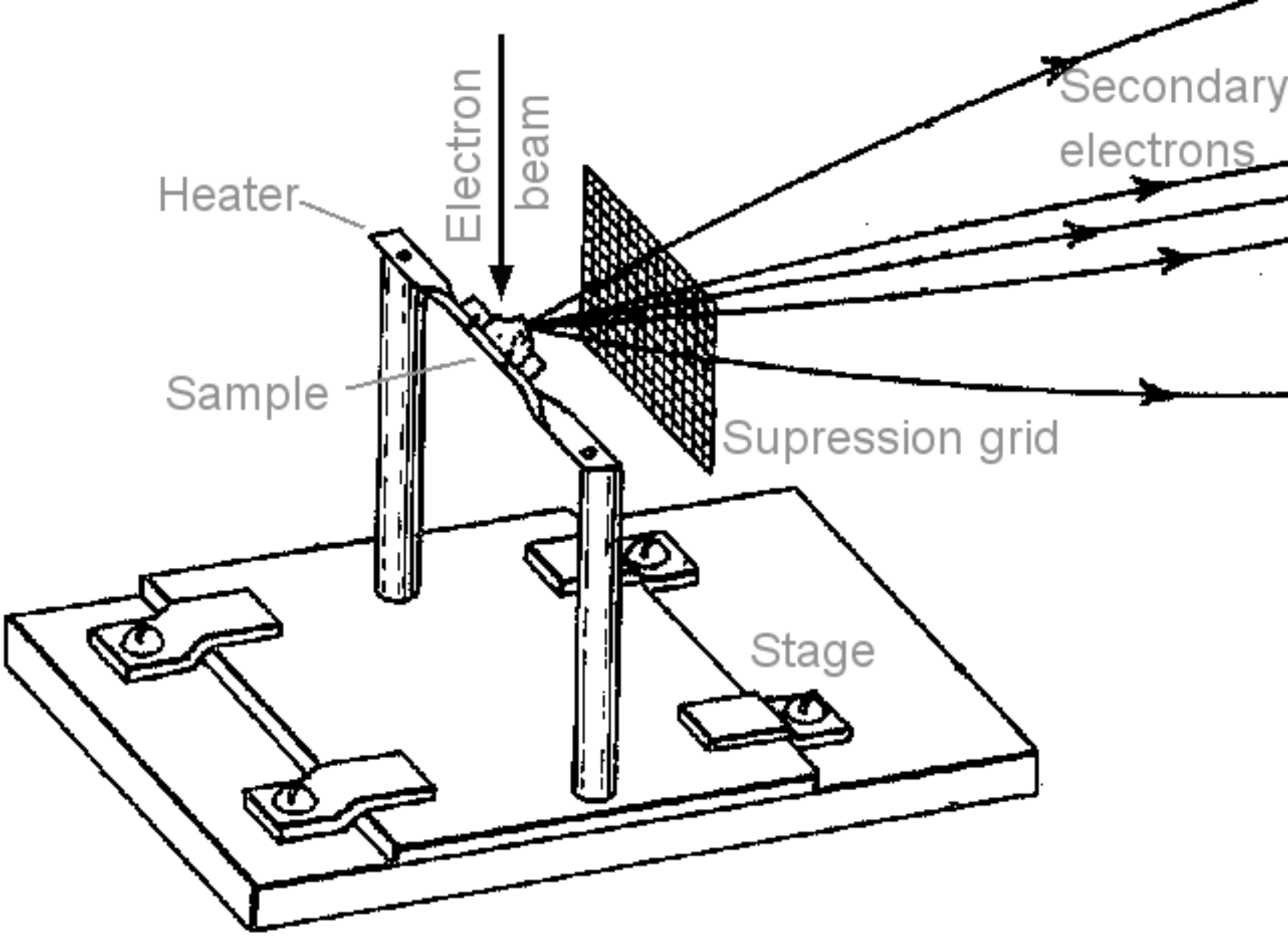
Electron beam
Secondary electrons
Heater
Sample
Supression grid
Stage

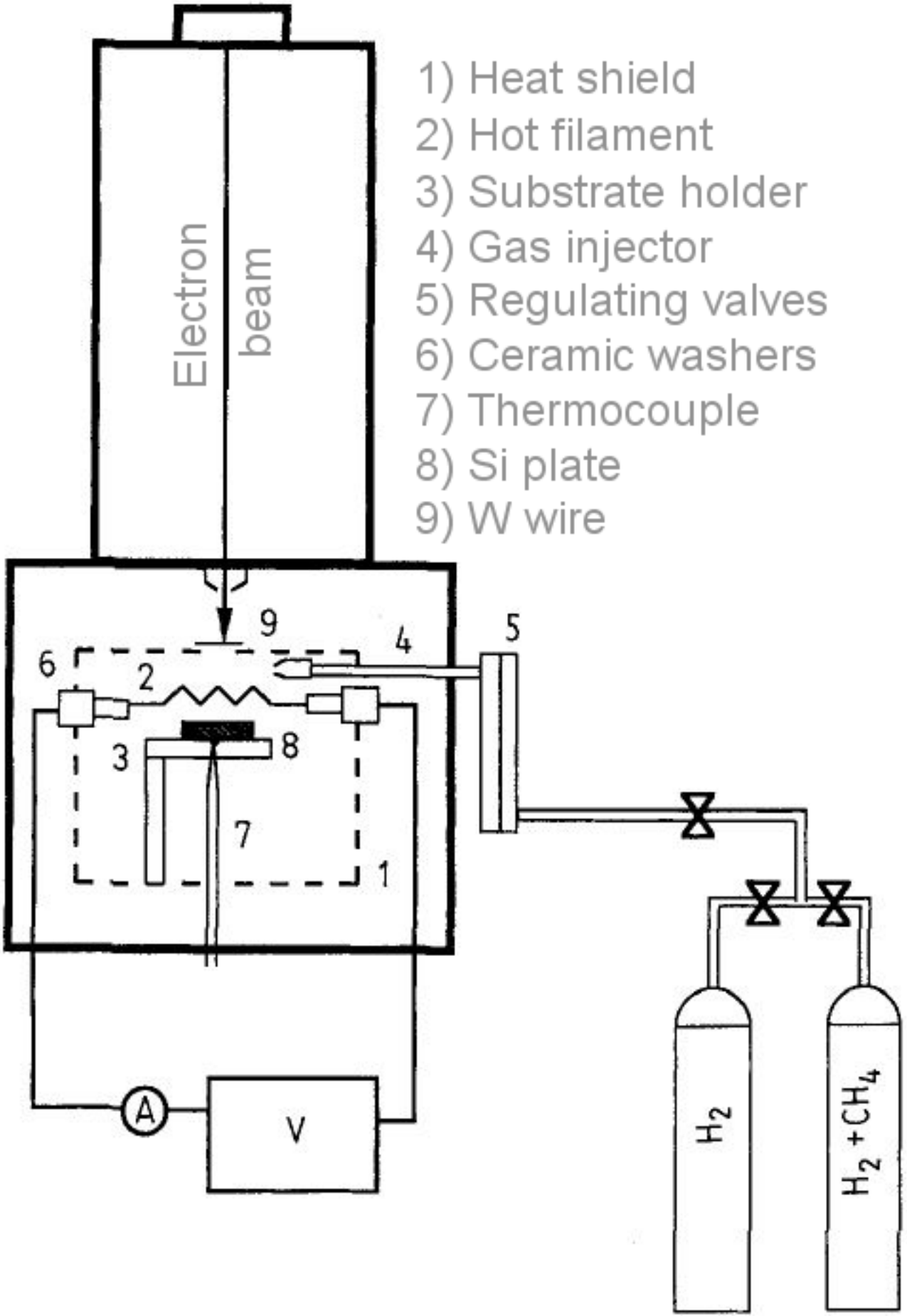
1) Heat shield
2) Hot filament
3) Substrate holder
4) Gas injector
5) Regulating valves
6) Ceramic washers
7) Thermocouple
8) Si plate
9) W wire
Electron beam
9
4
5
6
2
3
8
7
1
A
V
H_2
$H_2 + CH_4$

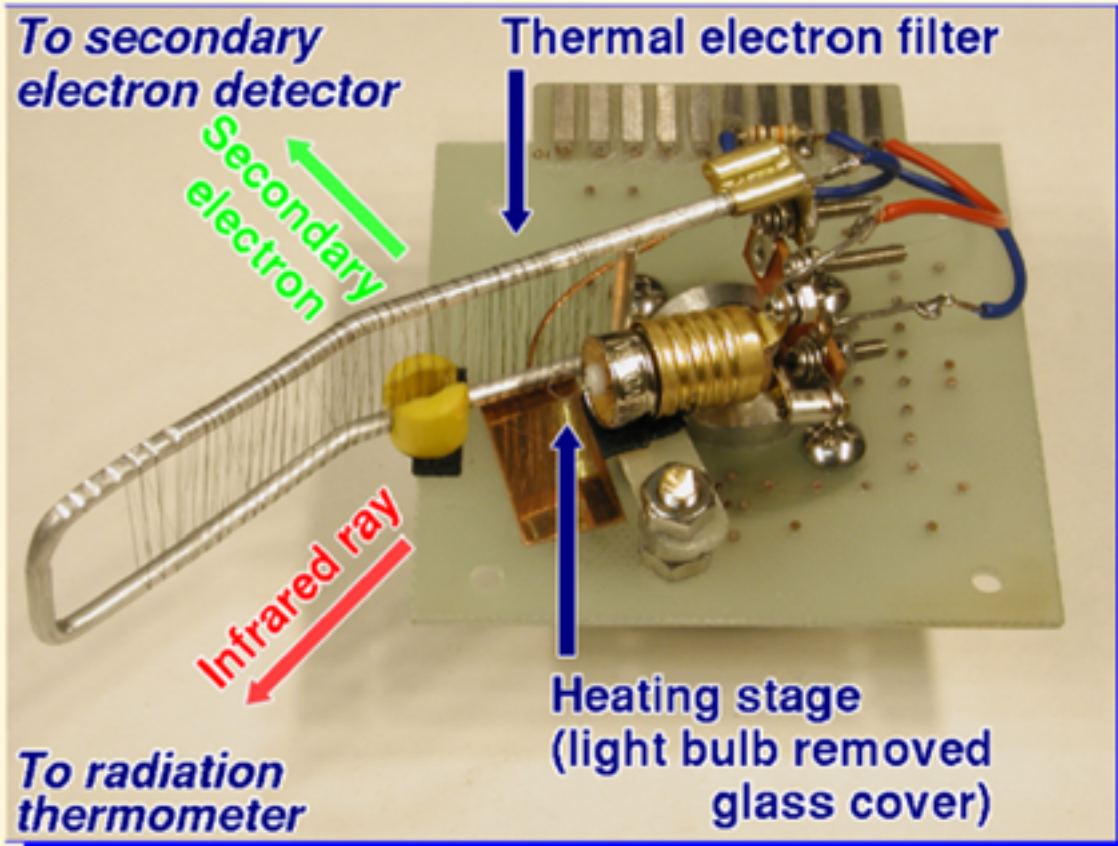
To secondary electron detector
Thermal electron filter
Secondary electron
Infrared ray
Heating stage (light bulb removed glass cover)
To radiation thermometer

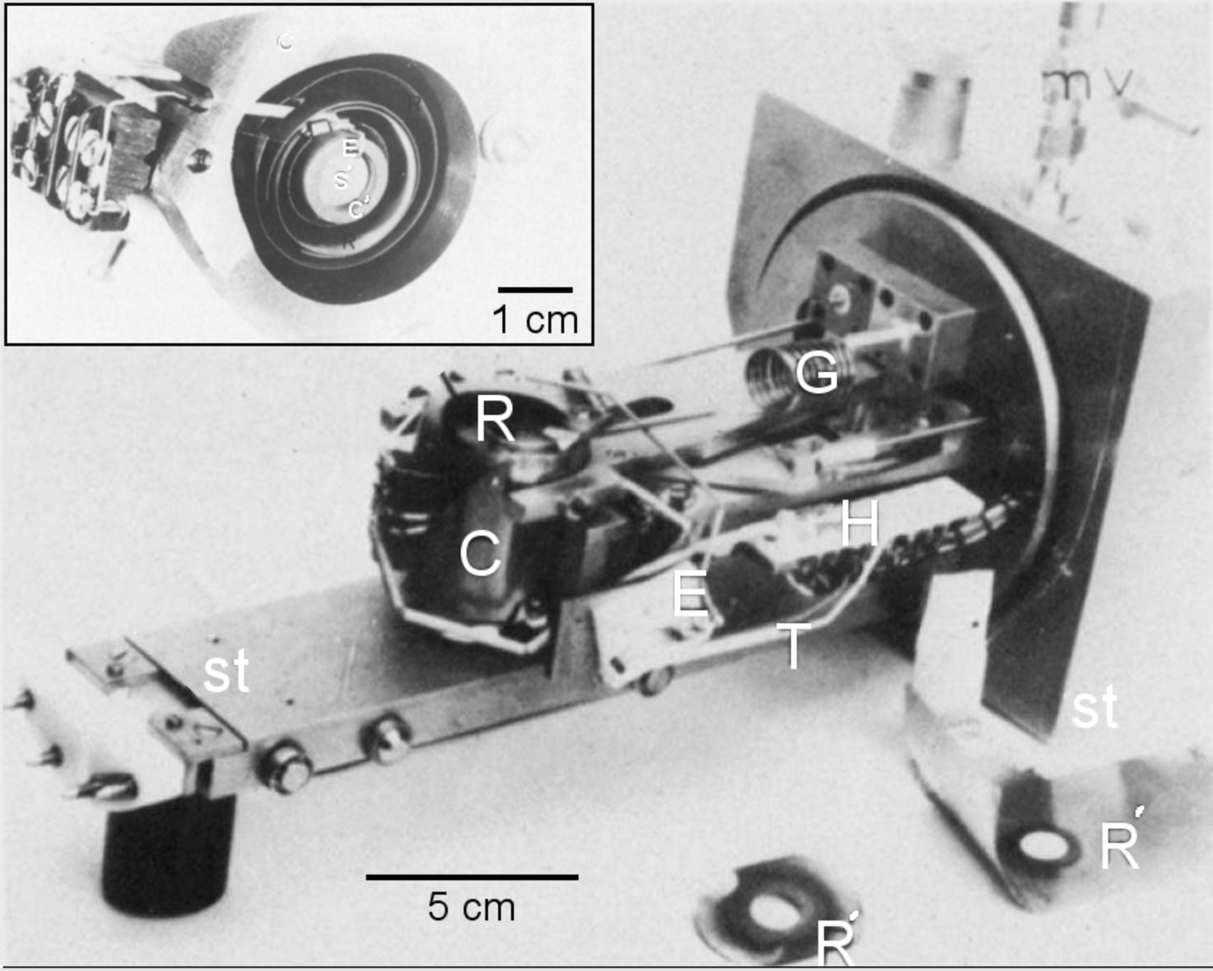

G: gas pipe
R: Radiation shield
E: Ground wire
T: Thermocouple wire
H: Heater wire

C: Cylinder
St: SEM Stage
C': Ceramic ring
S': Specimen

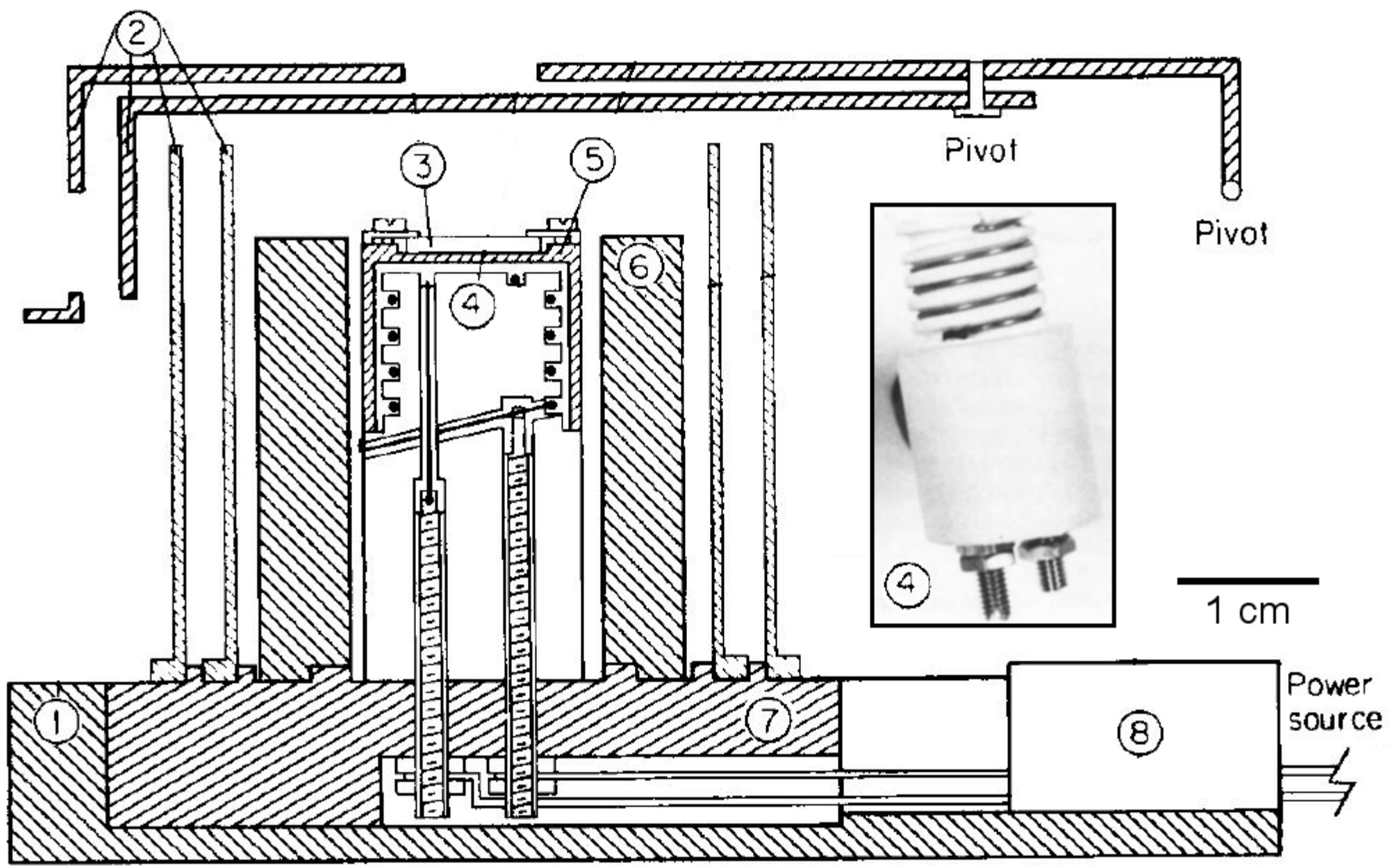

1) Stainless steel base
2) Stainless steel heat shield
3) Specimen
4) Heater
5) Specimen support
6) Pyrophyllite heat shield
7) Pyrophyllite base
8) Terminal block

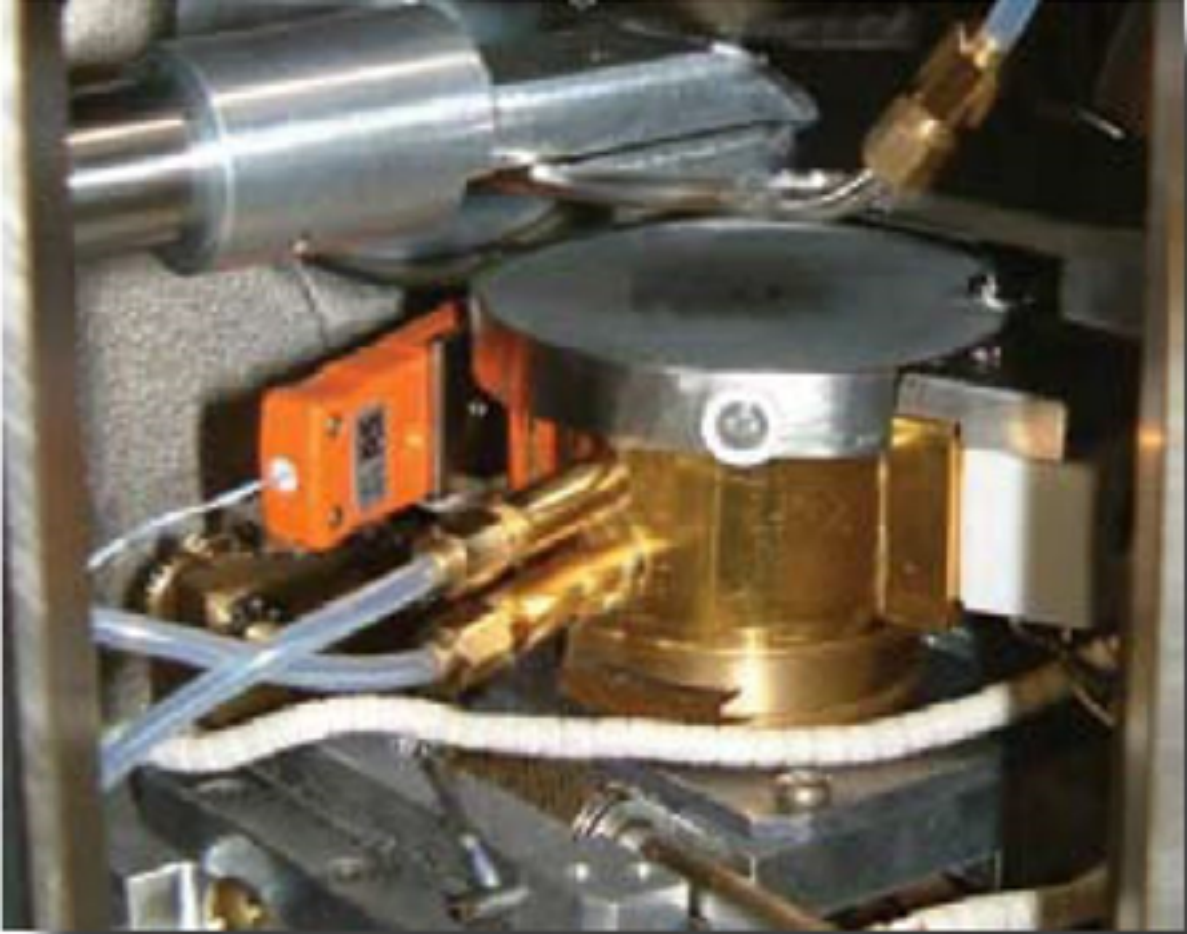

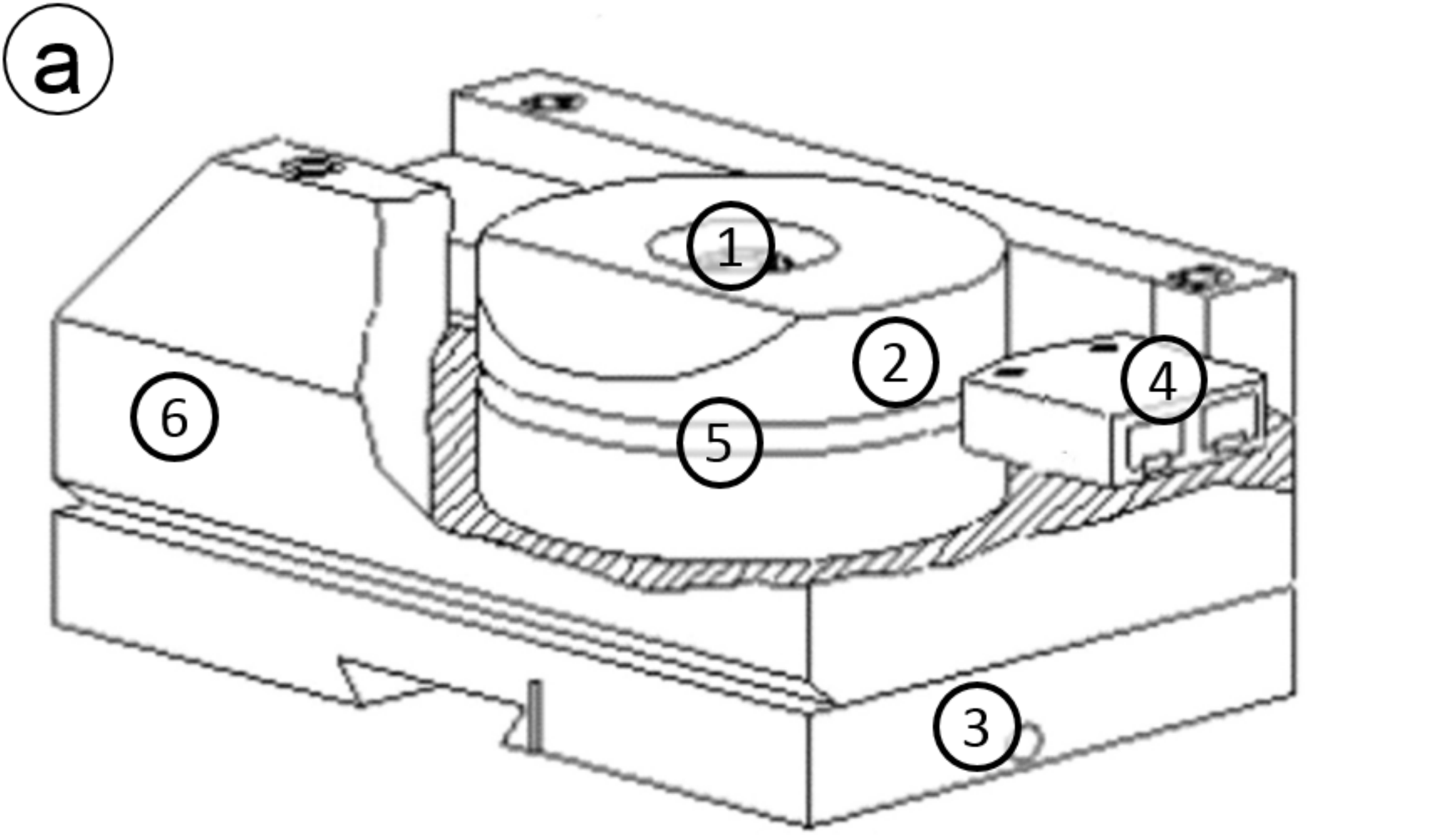

1. Sample holder; 2. HT insulating ceramic; 3. Connection for the sample bias; 4. Connection for sample heater; 5. Position of the thermocouple; 6. Metallic envelope

Connection for the GSED

b

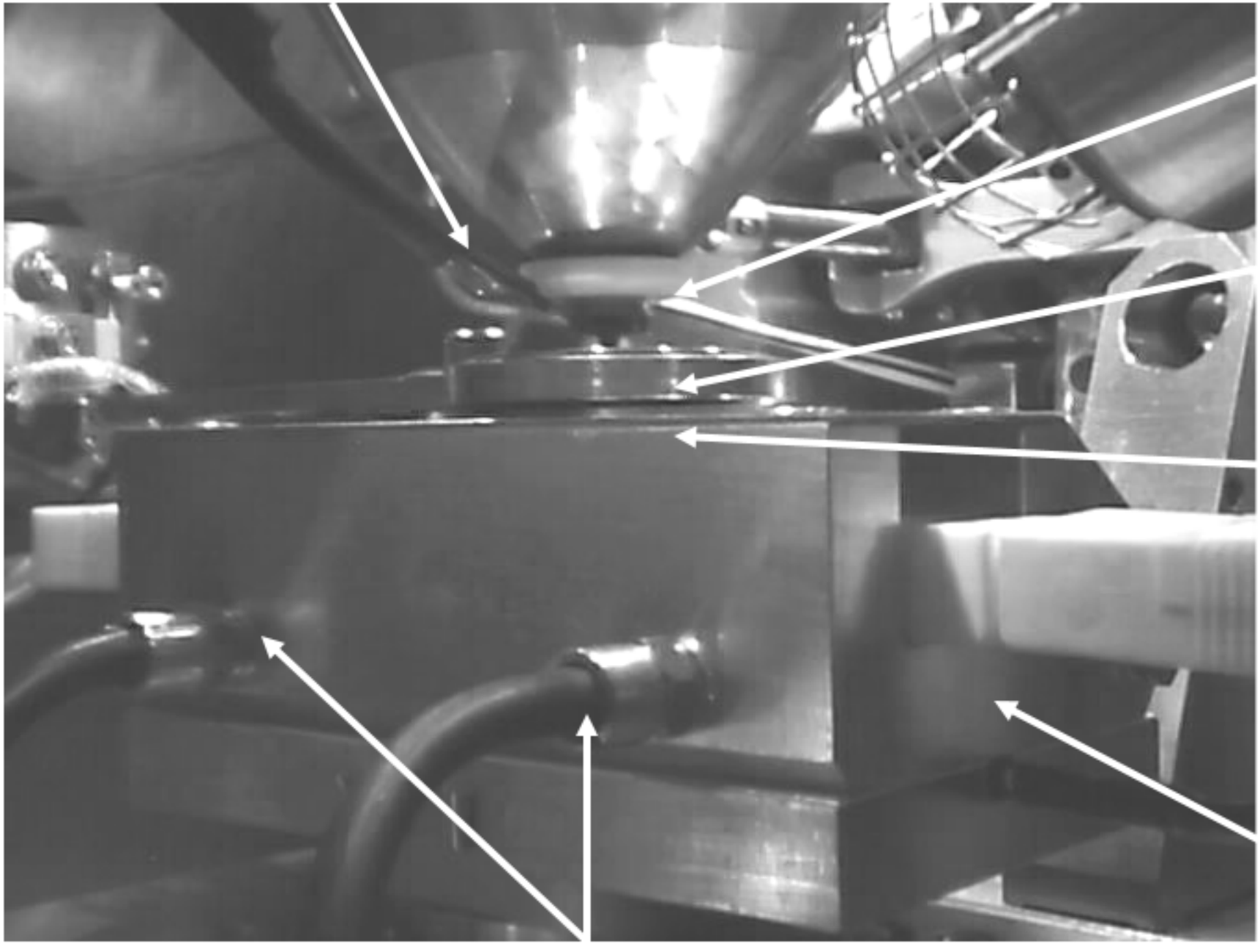

HT GSE detector

Heat shield

Sample holder

Sample bias

Cooling system

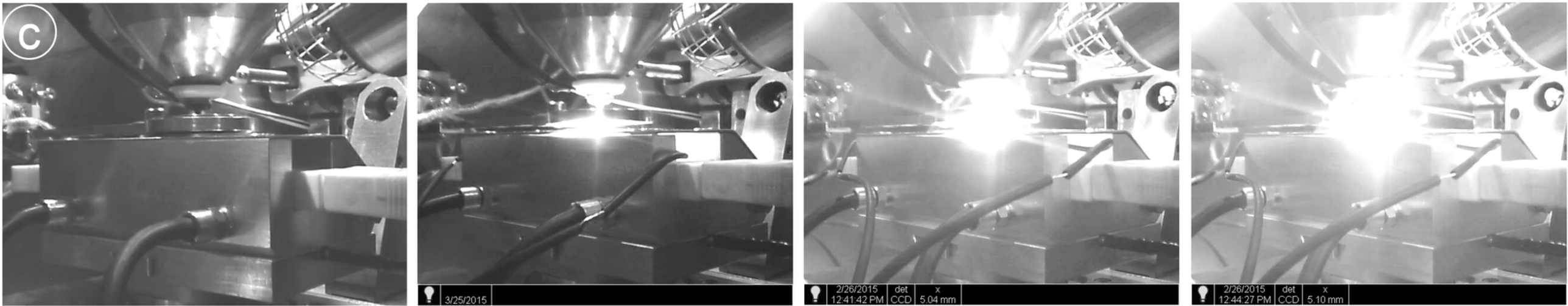
C
3/25/2015
2/26/2015
12:41:42 PM
det
CCD
x
5.04 mm
2/26/2015
12:44:27 PM
det
CCD
x
5.10 mm

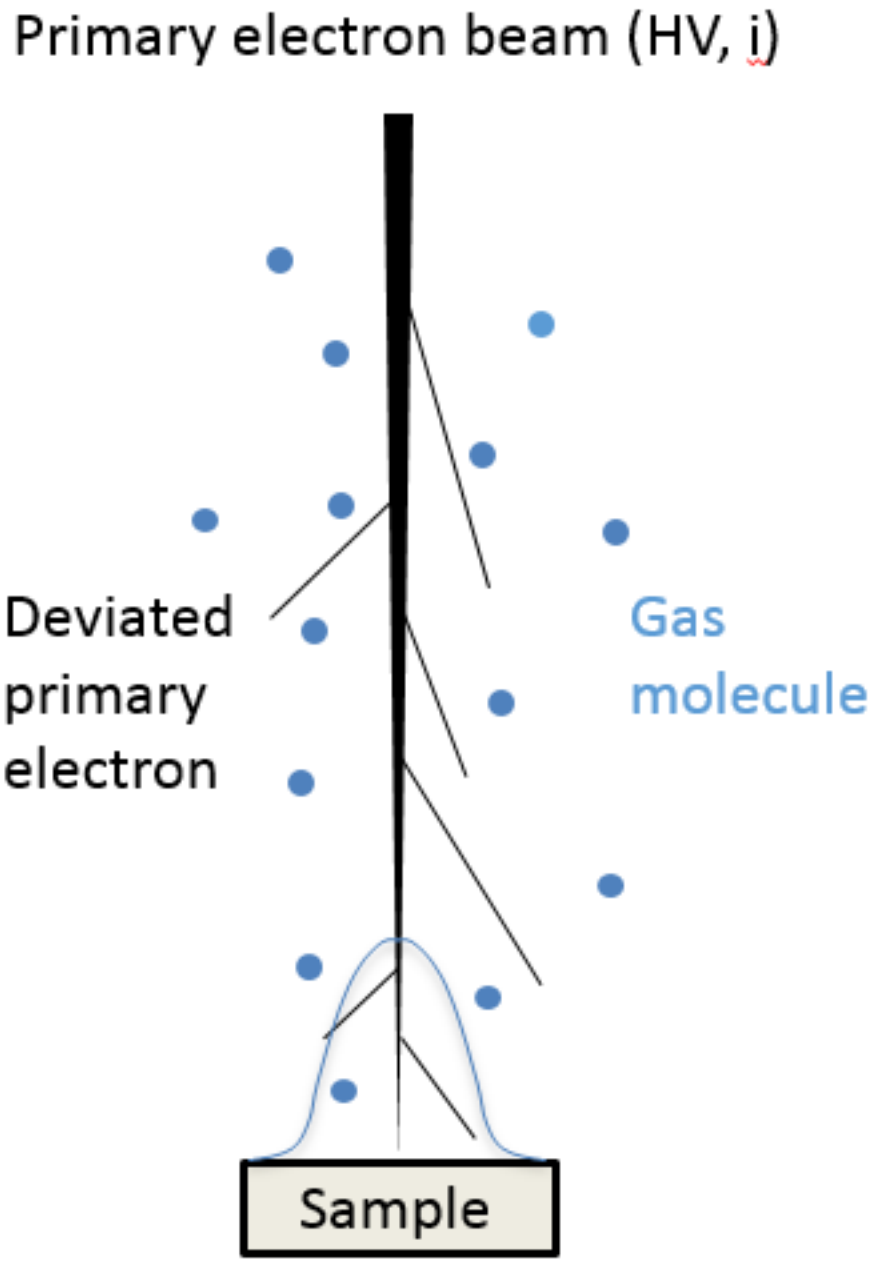

Skirt effect of the primary electron beam with the gas present in the ESEM chamber.

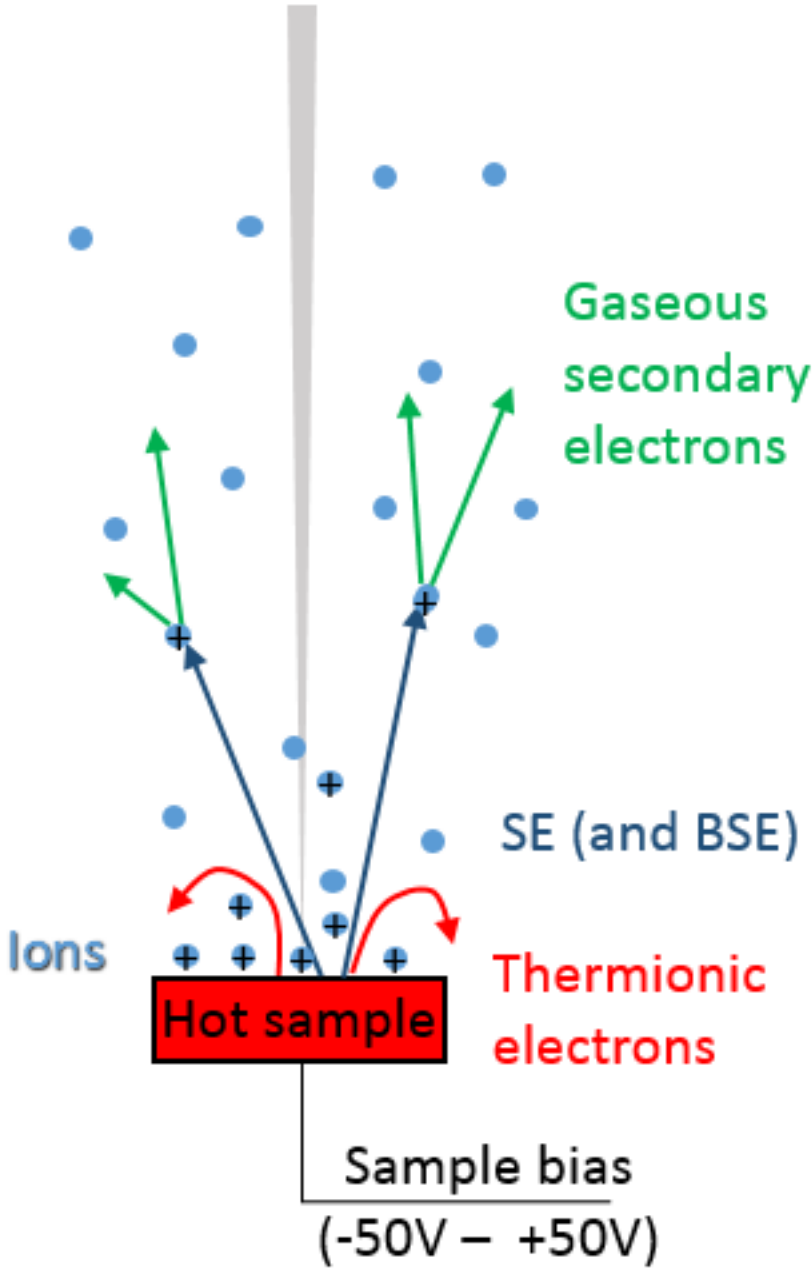

b) Electron signal amplification through successive cascade collisions of the SE/BSE with the gas molecules. Annihilation of surface charges by migration of the formed ions.

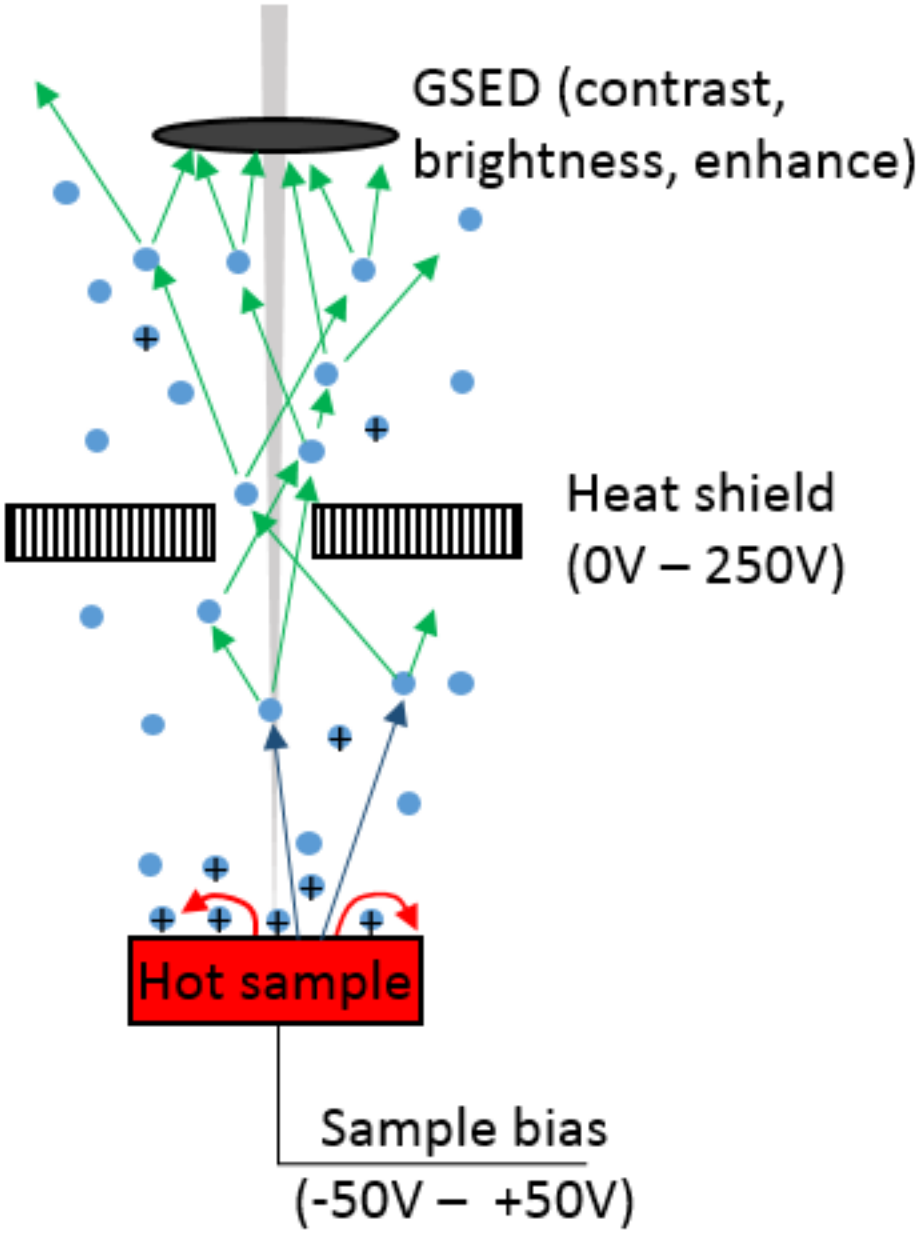

c) Acceleration of the SE by the heat shield and gaseous secondary electron collection by the GSED.

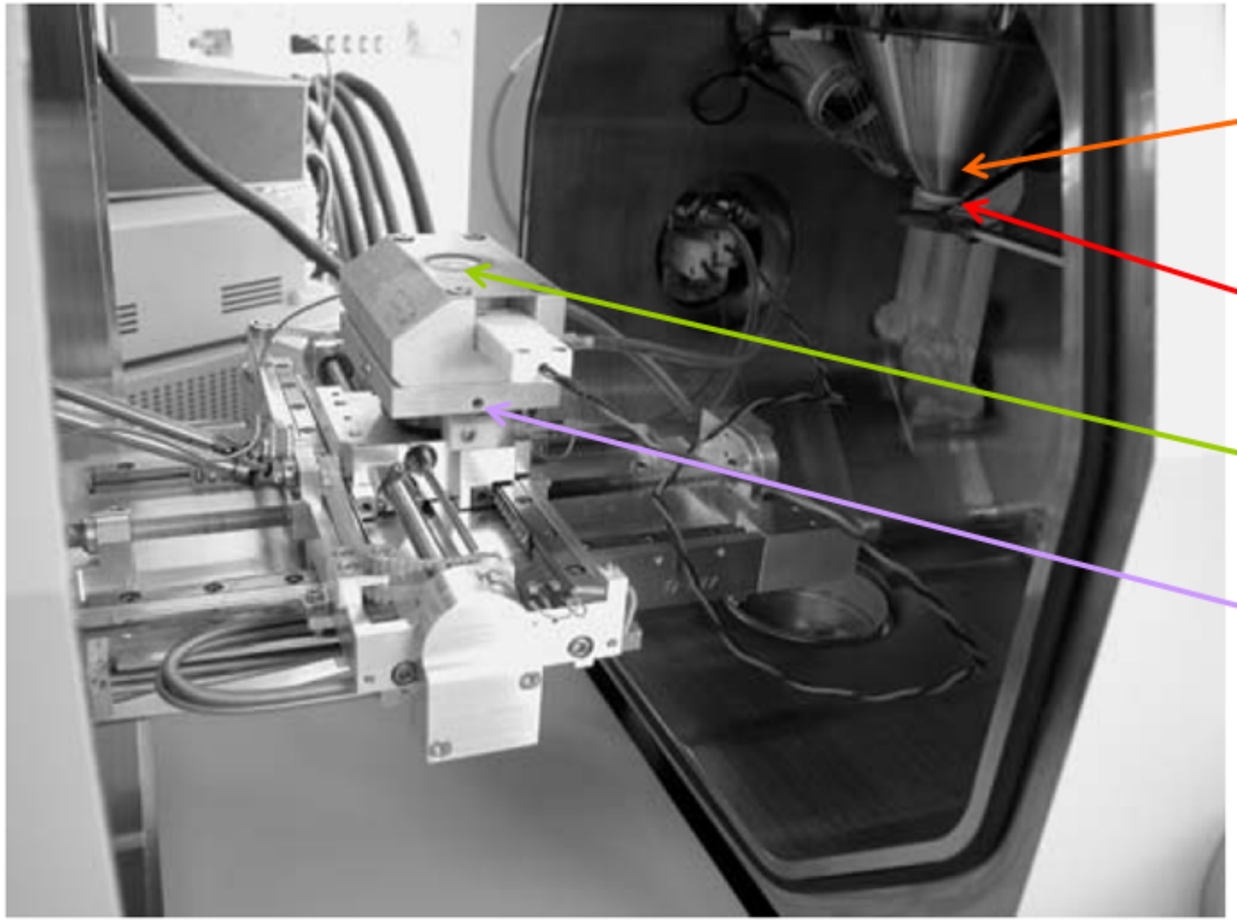

Electron Beam
([2]diaphragm diameter, [3]Acceleration voltage, [4]beam current, [5]working distance)

Image ([11]contrast, [12]brightness, [13]gamma)

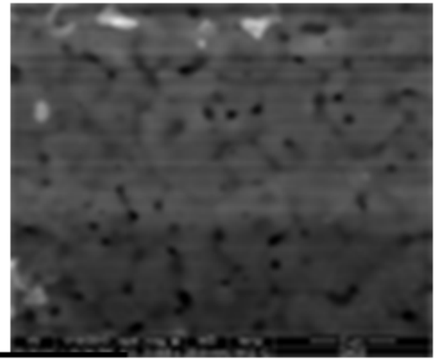

Detector
([6]contrast, [7]brightness, [8]enhance)

[1]Inner chamber pressure

[9]Heat shield (Bias)

[10]Sample Bias

- Biasing of the heat shield is inefficient
- The presence of the heat shield yields to a decrease of the number of electrons collected
- Remove the heat shield (up to 350°C)

- Biasing of the heat shield above 200V
- Increase of the image quality

- Increase of the intensity of the thermal electron emission
- Need for continuous adjusment of {contrast, brightness, enhance}

- Increase of the primary beam intensity (and HV)
- Modification of the parameters associated to the images {contrast, brightness, gamma}
- Decrease the heat shield bias

- The best range for the gas pressure is between 50 and 400Pa

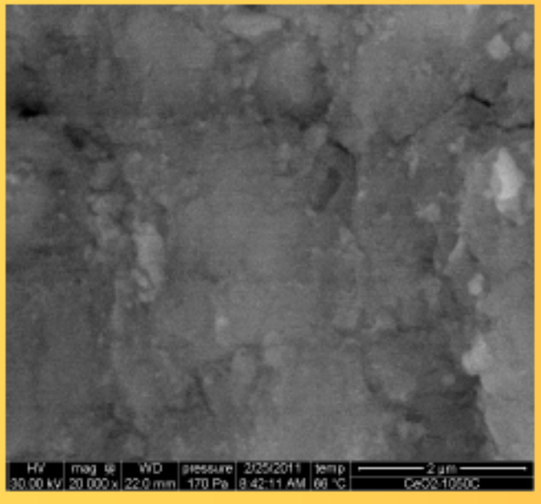

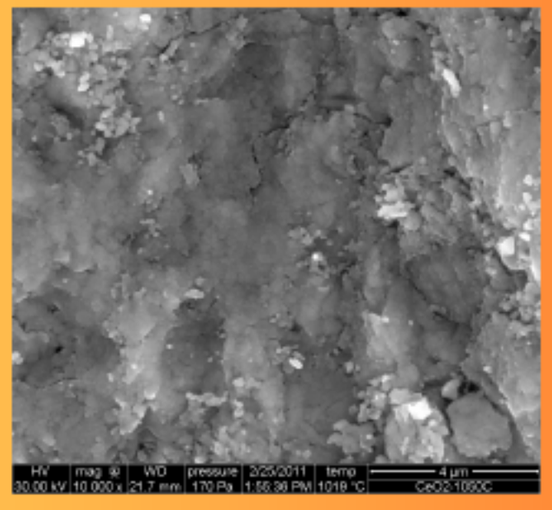

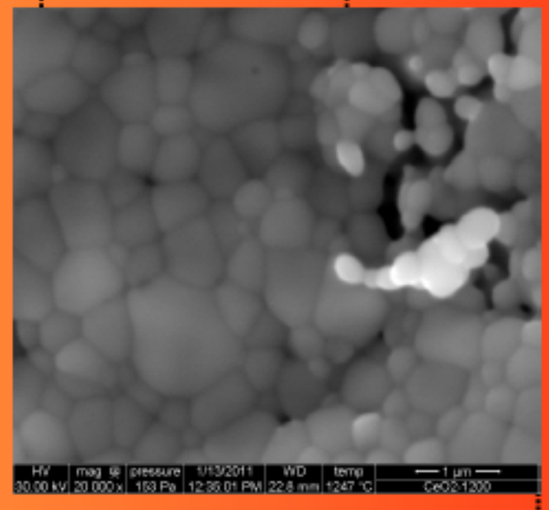

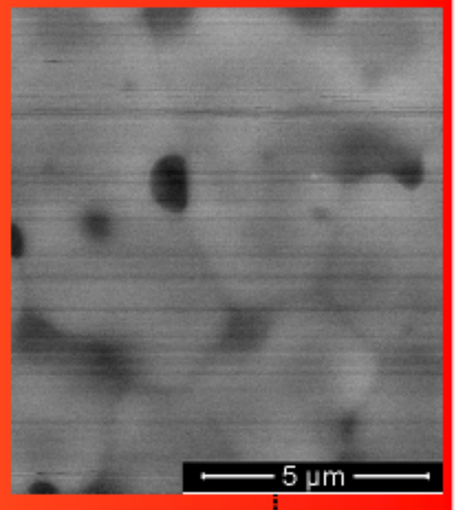

100°C 200°C 300°C 400°C 500°C 600°C 700°C 800°C 900°C 1000°C 1100°C 1200°C 1300°C 1400°C

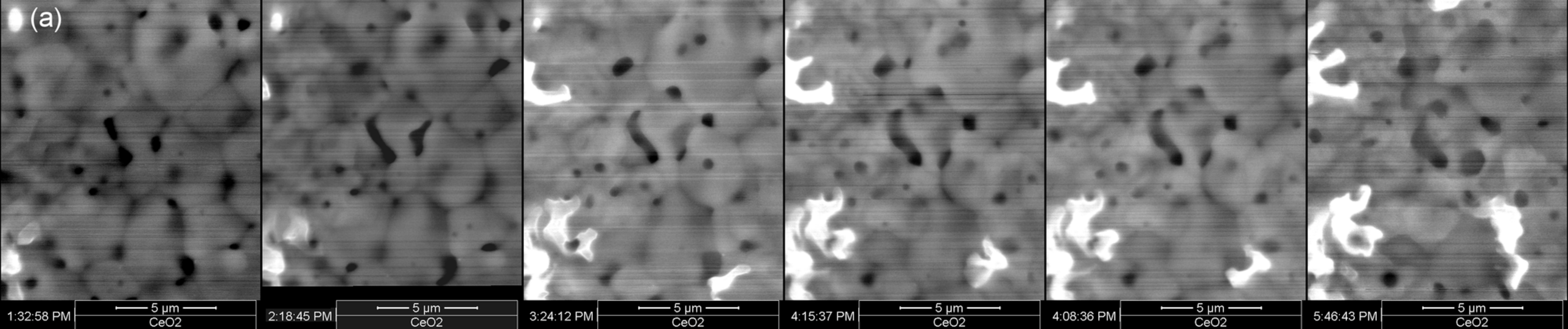
(a)
1:32:58 PM
5 µm
CeO2
2:18:45 PM
5 µm
CeO2
3:24:12 PM
5 µm
CeO2
4:15:37 PM
5 µm
CeO2
4:08:36 PM
5 µm
CeO2
5:46:43 PM
5 µm
CeO2

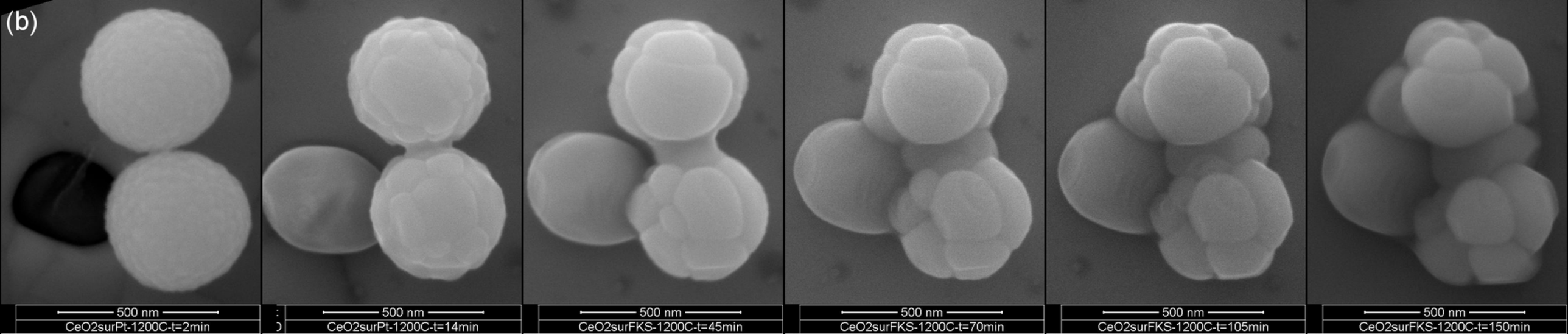
(b)
500 nm
CeO2surPt-1200C-t=2min
500 nm
CeO2surPt-1200C-t=14min
500 nm
CeO2surFKS-1200C-t=45min
500 nm
CeO2surFKS-1200C-t=70min
500 nm
CeO2surFKS-1200C-t=105min
500 nm
CeO2surFKS-1200C-t=150min

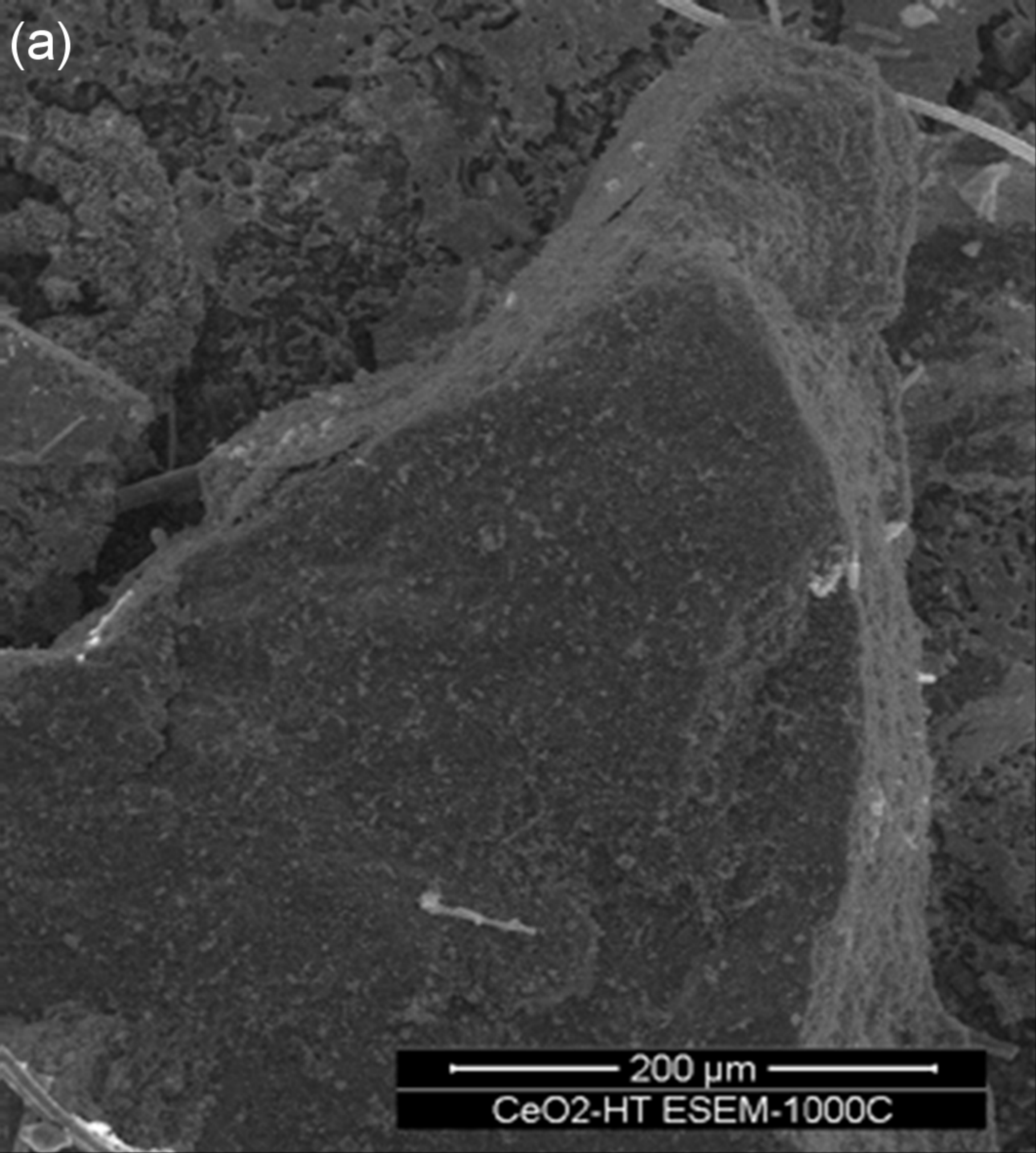
(a)
200 µm
CeO2-HT ESEM-1000C

(b)

5 μm

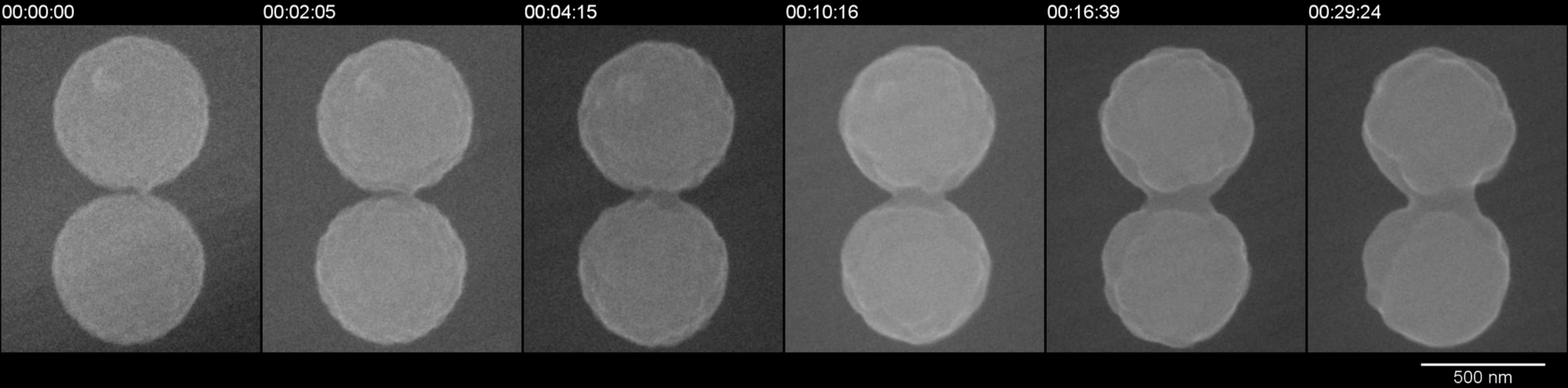
00:00:00
00:02:05
00:04:15
00:10:16
00:16:39
00:29:24
500 nm

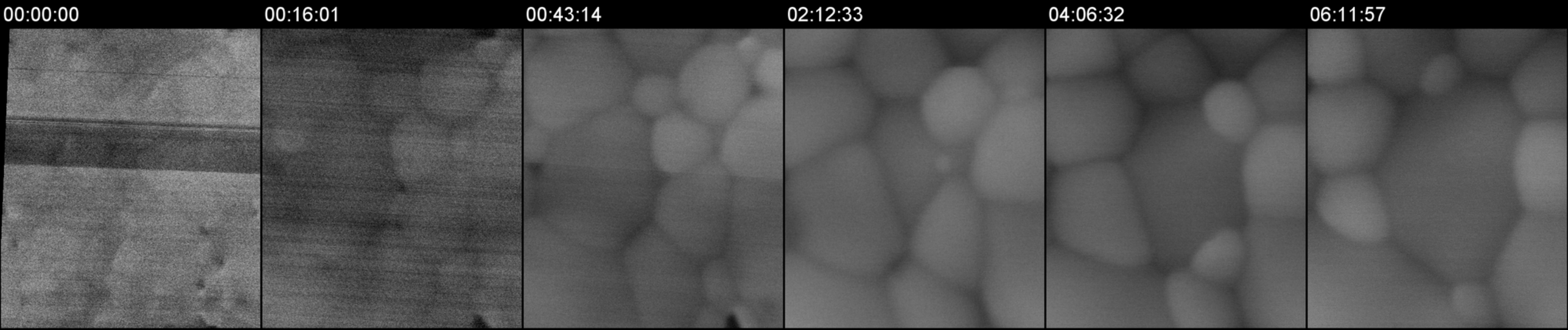
00:00:00
00:16:01
00:43:14
02:12:33
04:06:32
06:11:57
500 nm

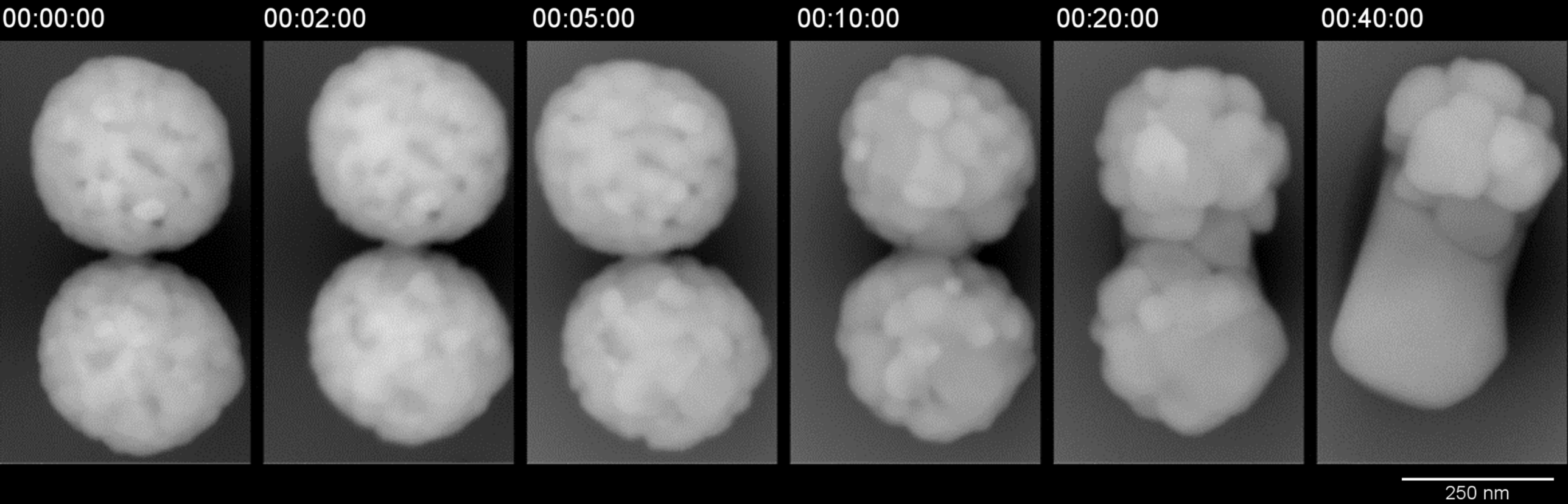
00:00:00
00:02:00
00:05:00
00:10:00
00:20:00
00:40:00
250 nm

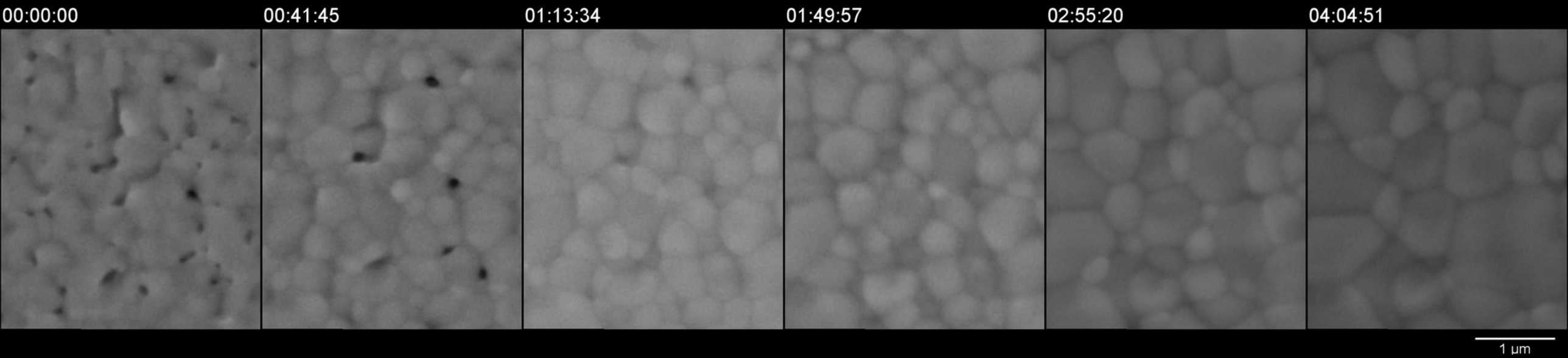
00:00:00
00:41:45
01:13:34
01:49:57
02:55:20
04:04:51
1 µm

(a)

mag	HV	WD	pressure	temp	2/10/2017	10 µm
2 500 x	20.00 kV	21.8 mm	80 Pa	850 °C	2:54:12 PM	Recrist VSH1 massif

(b)